Cell Metabolism

Article

Heterogenous impairment of α cell function in type 2 diabetes is linked to cell maturation state

Graphical abstract

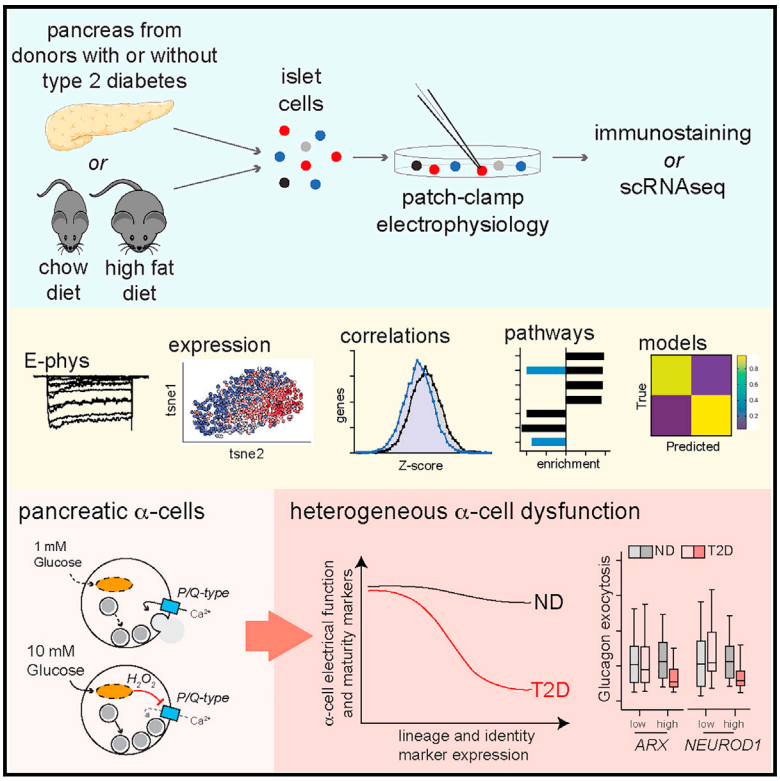

Highlights

- Glucose suppresses α cell exocytosis by inhibiting P/Q-type Ca^{2+} currents
- Patch-seq links maturation, respiration, and receptor expression to α cell function
- Dysfunction of α cells associates with a "β cell-like" electrophysiological signature
- Impaired exocytosis occurs in α cells enriched for lineage and immaturity markers

Authors

Xiao-Qing Dai, Joan Camunas-Soler, Linford J.B. Briant, ..., Roland W. Stein, Stephen R. Quake, Patrick E. MacDonald

Correspondence

pmacdonald@ualberta.ca

In brief

In diabetes, glucagon secretion from pancreatic α cells is dysregulated. Dai et al. examined electrical and transcriptomic α cell phenotypes and found that dysfunction in type 2 diabetes is linked to cell maturation state and impaired α cell identity. Notably, a subset of α cells enriched for lineage markers appears uniquely susceptible to dysfunction.

Dai et al., 2022, Cell Metabolism *34*, 256–268
February 1, 2022
https://doi.org/10.1016/j.cmet.2021.12.021

CellPress

CellPress
OPEN ACCESS

Cell Metabolism

Article

Heterogenous impairment of α cell function in type 2 diabetes is linked to cell maturation state

Xiao-Qing Dai,[1,2,14] Joan Camunas-Soler,[3,4,14] Linford J.B. Briant,[5] Theodore dos Santos,[1,2] Aliya F. Spigelman,[1,2] Emily M. Walker,[6] Rafael Arrojo e Drigo,[7] Austin Bautista,[2] Robert C. Jones,[3] Dana Avrahami,[8] James Lyon,[2] Aifang Nie,[1,2] Nancy Smith,[1,2] Yongneng Zhang,[9] Janyne Johnson,[1,2] Jocelyn E. Manning Fox,[1,2] Evangelos D. Michelakis,[9] Peter E. Light,[1,2] Klaus H. Kaestner,[10] Seung K. Kim,[11,12] Patrik Rorsman,[5] Roland W. Stein,[7] Stephen R. Quake,[3,4,13] and Patrick E. MacDonald[1,2,15,16,17,*]

[1]Department of Pharmacology, University of Alberta, Edmonton, AB T6G2R3, Canada
[2]Alberta Diabetes Institute, University of Alberta, Edmonton, AB T6G2R3, Canada
[3]Department of Bioengineering, Stanford University, Stanford, CA 94305, USA
[4]Chan Zuckerberg Biohub, San Francisco, CA 94518, USA
[5]Oxford Centre for Diabetes, Endocrinology and Metabolism, Radcliffe Department of Medicine, Churchill Hospital, Oxford OX3 7LE, UK
[6]Department of Internal Medicine, University of Michigan, Ann Arbor, MI 48105, USA
[7]Department of Molecular Physiology and Biophysics, Vanderbilt University Medical Center, Nashville, TN, USA
[8]Endocrinology and Metabolism Department, Hadassah-Hebrew University Medical Centre, Jerusalem, Israel
[9]Department of Medicine, University of Alberta, Edmonton, AB T6G2R3, Canada
[10]Department of Genetics and Institute for Diabetes, Obesity and Metabolism, Perelman School of Medicine, University of Pennsylvania, Philadelphia, PA 19104, USA
[11]Department of Developmental Biology, Stanford University School of Medicine, Stanford, CA 94305, USA
[12]Stanford Diabetes Research Center, Stanford University, Stanford, CA 94305, USA
[13]Department of Applied Physics, Stanford University, Stanford, CA 94305, USA
[14]These authors contributed equally
[15]Present address: Alberta Diabetes Institute, LKS Centre, Rm. 6-126, University of Alberta, Edmonton, AB T6G 2R3, Canada
[16]Twitter: @bcellorg
[17]Lead contact
*Correspondence: pmacdonald@ualberta.ca
https://doi.org/10.1016/j.cmet.2021.12.021

SUMMARY

In diabetes, glucagon secretion from pancreatic α cells is dysregulated. The underlying mechanisms, and whether dysfunction occurs uniformly among cells, remain unclear. We examined α cells from human donors and mice using electrophysiological, transcriptomic, and computational approaches. Rising glucose suppresses α cell exocytosis by reducing P/Q-type Ca^{2+} channel activity, and this is disrupted in type 2 diabetes (T2D). Upon high-fat feeding of mice, α cells shift toward a "β cell-like" electrophysiological profile in concert with indications of impaired identity. In human α cells we identified links between cell membrane properties and cell surface signaling receptors, mitochondrial respiratory chain complex assembly, and cell maturation. Cell-type classification using machine learning of electrophysiology data demonstrated a heterogenous loss of "electrophysiologic identity" in α cells from donors with type 2 diabetes. Indeed, a subset of α cells with impaired exocytosis is defined by an enrichment in progenitor and lineage markers and upregulation of an immature transcriptomic phenotype, suggesting important links between α cell maturation state and dysfunction.

INTRODUCTION

In concert with reduced insulin secretion from pancreatic β cells in type 2 diabetes (T2D), disrupted glucagon secretion from α cells contributes to hyperglycemia and impaired hypoglycemia counter-regulation (Girard, 2017). While insulin and glucagon secretion are both dependent on electrical excitability and Ca^{2+}-dependent exocytosis, the nature of the ion channels involved and their roles and the impact of glucose-stimulation differ in α and β cells. Insulin granule exocytosis is linked to Ca^{2+} entry via L-type Ca^{2+} channels, whereas glucagon secretion is coupled to P/Q-type Ca^{2+} channels (De Marinis et al., 2010). Also, Na^+ channels play a more prominent role in glucagon secretion (Barg et al., 2000; Göpel et al., 2000; Ramracheya et al., 2010) and differ in their regulation between these cell types (Zhang et al., 2014). In rodents, such differences can distinguish α from β cells, either by Na^+ current properties (Zhang et al., 2014) or "electrophysiological fingerprints" (Briant et al., 2017).

Similar to β cells, the excitatory and secretory machinery in α cells, including ion channel activities (Huang et al., 2011a),

Ca^{2+} responses (Le Marchand and Piston, 2010; Reissaus and Piston, 2017; Shuai et al., 2016), glucagon content (Zadeh et al., 2020), and exocytotic capacity (Huang et al., 2011b), is heterogeneous. Indeed, the intracellular Ca^{2+} response of α cells varies, with some suppressed by glucose and others activated (Shuai et al., 2016). This suggests a heterogeneity among these cell types, which is supported by single-cell transcriptomics (Camunas-Soler et al., 2020; Korsunsky et al., 2019). Recent reports suggest a subpopulation of α cells (or "α-like cells") that are proliferative. In mice these are identified by *Slc38a5*, which encodes an amino acid transporter (Kim et al., 2017); in humans these may be identified by the presence of ARX and cytosolic Sox9 (Lam et al., 2018). These cells could account for α cell hyperplasia upon glucagon-receptor antagonism and may be a source of new β cells (van der Meulen et al., 2017).

While little evidence so far suggests that α cells dedifferentiate in diabetes, they can trans-differentiate in rodents following severe β cell loss (Thorel et al., 2010) or genetic manipulation of transcription factor expression (Chakravarthy et al., 2017; Matsuoka et al., 2017). Interestingly, α cells may show more plasticity than β cells (Bramswig et al., 2013), as they appear to exist in distinct states characterized by chromatin accessibility at promotors for *GCG*, functional genes such as *ABCC8*, and at sites enriched in motifs for transcription factors of the RFX, GATA, and NEUROD families, among others (Chiou et al., 2021). In type 1 diabetes, the expression of α cell markers is reduced (Brissova et al., 2018) and in T2D α cells express an immature transcriptomic profile (Avrahami et al., 2020).

We hypothesized that this plasticity influences α cell membrane function, contributing to dysfunction in T2D. We used correlated electrophysiological and single-cell RNA seq (patch-seq) of α cells from human donors and mice to define a cell-autonomous glucose regulation of α cell Ca^{2+} channel activity and exocytosis that is associated with α cell maturation state and identified putative regulators of glucagon secretion. These include the mitochondrial respiratory chain complex and numerous cell surface receptors. In mice, high-fat feeding prompts some α cells to adopt a "β cell-like" electrical profile and impaired identity. Similarly, in human T2D, α cells enriched for markers of mitochondrial function and endocrine lineage such as *NEUROD1*, *ISL1*, *NKX2-2*, and *ARX* exhibit a selective induction of an immature transcriptional profile, impaired electrophysiological phenotype, and dysregulated exocytosis. This suggests an important link between α cell maturation, identity, and dysfunction in T2D.

RESULTS

Glucose-mediated suppression of α cell exocytosis is disrupted in T2D

In β cells, glucose metabolism amplifies Ca^{2+}-triggered exocytosis and insulin secretion (Ferdaoussi et al., 2015; Gembal et al., 1992; Sato et al., 1992), which is linked to the activation of L-type Ca^{2+} channels (Barg et al., 2001; Bokvist et al., 1995; Wiser et al., 1999). We examined the impact of glucose on glucagon exocytosis in α cells from donors with no diabetes (ND) or with T2D (Table S1) following dispersion to single cells and identification by glucagon immunostaining (Figure 1A). In ND α cells, exocytosis was highest at low glucose (1 mM) and was suppressed by increasing glucose (to 5–20 mM) (Figures 1B and S1). In α cells from donors with T2D, exocytosis was ~75% lower at 1 mM glucose than in α cells from ND donors, and elevating glucose levels exerted a modest increase (Figures 1B and S1A). The differences between ND and T2D cells, also seen when grouped by donor (Figure S1B), are consistent with a recent live-cell imaging study (Omar-Hmeadi et al., 2020). In ND α cells, voltage-dependent Ca^{2+} channel activity was lower at elevated glucose than in α cells from donors with T2D, here recorded using Ba^{2+} as a charge carrier (Figures 1C and S1C), and the relationship between Ca^{2+} entry and exocytosis was not altered (Figure S1D).

The majority of the human α cell Ca^{2+} current is mediated by L-type and P/Q-type channels (Ramracheya et al., 2010), and the latter are directly linked to glucagon exocytosis (Dai et al., 2014; Ramracheya et al., 2010, 2018). The low α cell exocytosis at elevated glucose could be reversed by the P/Q-type Ca^{2+} channel activator GV-58 (Tarr et al., 2012), which delays Ca^{2+} current inactivation (Figure 1D). The P/Q-type channel blocker agatoxin inhibited exocytosis from ND α cells at 1 mM glucose while the L-type channel blocker isradipine did not (Figure 1E). Finally, the greater P/Q-type Ca^{2+} channel activity seen in ND α cells at 1 mM glucose was largely absent in T2D (Figures 1F and S1A) but still contributed to the modest glucose-dependent increase in exocytosis (Figure 1G). Thus, in ND α cells increasing glucose inhibits P/Q-type Ca^{2+} channels to limit exocytosis, an effect that requires intact mitochondrial function (Figures S1E and S1F). In T2D α cells, Ca^{2+} channel activity at low glucose is reduced and increasing glucose facilitates exocytosis (Figure 1H).

Patch-seq highlights a role for the mitochondrial respiratory chain in α cell exocytosis and suggests poor responsiveness in immature α cells

We performed patch-seq in α cells, some initially pre-incubated at low glucose for 1 h. However, exocytosis was low after an extended time at 1 mM glucose due to depletion of glucagon granules (Figure S2). These pre-incubated cells were excluded from further analysis, and we performed transcriptome-wide correlations with exocytosis in 400 human α cells (from 31 donors) exposed acutely to 1 and 10 mM glucose (Figure 2A). ND α cells at 1 mM were enriched for positively correlated genes while negatively correlated genes were enriched at 10 mM glucose (Figure 2B; Table S2). Gene set enrichment analysis (GSEA) using *Z* scores of transcripts found in >20% of cells highlighted pathways associated with elevated α cell exocytosis at 1 mM glucose and lower exocytosis at 10 mM glucose (Figure 2C). Consistent with a role for metabolism in determining α cell responsiveness, we found mitochondrial respiratory chain complex assembly as a positive correlate to exocytosis at low glucose and a negative correlate at high glucose (Figures 2C and 2D). A separate over-representation analysis (ORA) yielded similar results, highlighting the electron transport chain in the glucose regulation of α cell exocytosis (Figure S3A).

Ca^{2+} channel transcripts were not reduced in α cells of T2D donors compared with those from ND donors (Figures S3B and S3C). Hyperglycemia may induce α cell mitochondrial dysfunction (Knudsen et al., 2019), and we saw a modest but

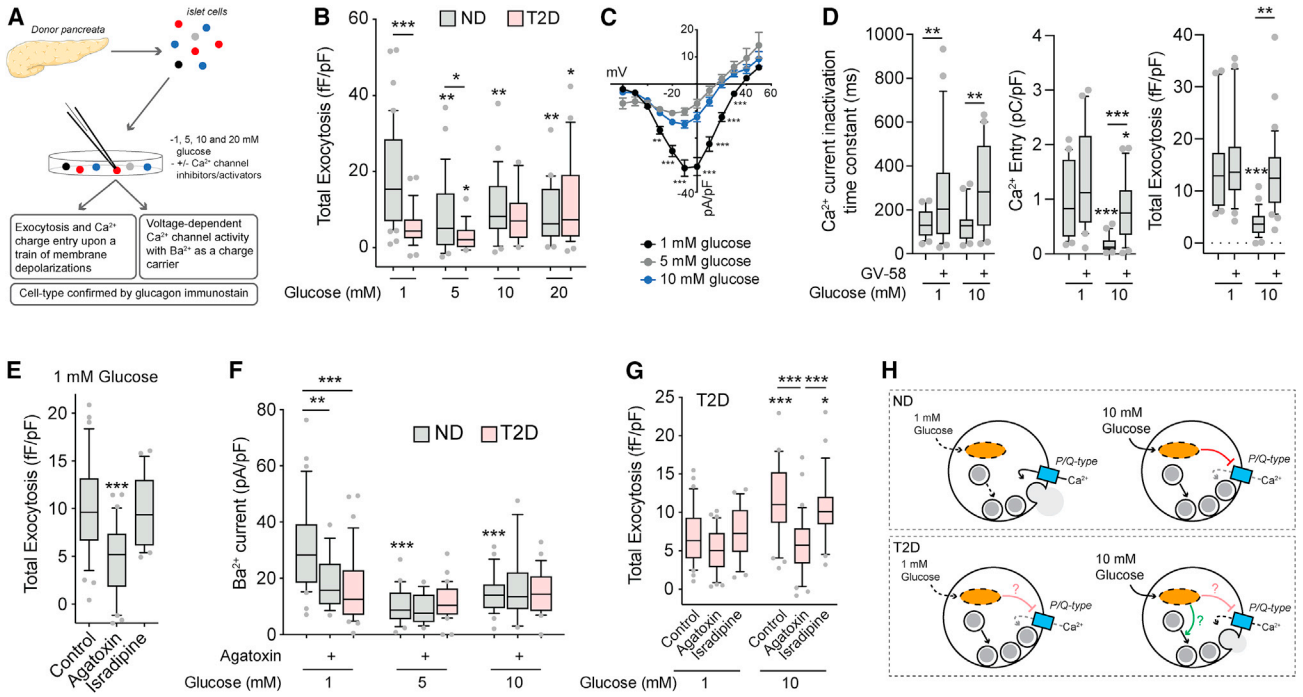

Figure 1. Glucose suppresses human α cell exocytosis in concert with P/Q-channel activity

(A) Schematic diagram illustrating that human islets were isolated, dispersed, and cultured for 1–2 days prior to whole-cell patch-clamp and subsequent α cell identification by glucagon immunostaining.

(B) Total exocytosis upon a series of ten membrane depolarizations with increasing glucose in ND α cells (gray; n = 42, 28, 24, 20 cells from 9 donors) and T2D α cells (pink; n = 29, 16, 12, 27 cells from 6 donors).

(C) Voltage-dependent Ca^{2+} channel activity with Ba^{2+} as a charge carrier in ND α cells with increasing glucose (n = 31, 24, 27 cells from 7 donors).

(D) Effect of the P/Q-type Ca^{2+} channel activator GV-58 (10 μM) on Ca^{2+} current inactivation (left; n = 24, 28, 22, 21 cells) and charge entry (middle; n = 22, 20, 20, 23 cells) during a 500 ms depolarization from − 70 to 0 mV and total exocytosis (right; n = 23, 22, 28, 34 cells) at 1 and 10 mM glucose (3 donors).

(E) Effect of the P/Q-type Ca^{2+} channel blocker agatoxin (100 nM) and the L-type Ca^{2+} channel blocker isradipine (10 μM) on exocytosis at 1 mM glucose in ND α cells (n = 34, 30, 21 cells from 5 donors).

(F) Voltage-dependent Ca^{2+} channel activity at 0 mV (Ba^{2+} as a charge carrier) with increasing glucose in ND α cells, with agatoxin (100 nM), and in T2D α cells (n = 31, 16, 24, 15, 27, 18 cells from 7 ND donors and 34, 31, 27 cells from 5 T2D donors).

(G) Effect of agatoxin (100 nM) and the L-type Ca^{2+} channel blocker isradipine (10 μM) on total exocytosis in T2D α cells at 1 and 10 mM glucose (n = 30, 31, 29, 32, 31, 29 cells from 5 T2D donors).

(H) Putative scheme for glucose regulation of depolarization-induced exocytosis in α cells and the dysfunction seen in T2D.

*p < 0.05; **p < 0.01; ***p < 0.001 by one-way ANOVA (D, E, and G) or two-way ANOVA (B, C, and F) and Tukey post test compared with 1 mM glucose control, or as indicated.

significantly higher mitochondrial respiratory chain complex transcript expression in α cells of T2D donors compared with α cells from ND donors (Figures S3D and S3E). Intriguingly, transcripts associated with endocrine development appeared as anti-correlates of exocytosis at 1 mM glucose (Figures 2C, 2E, and 2F), suggesting a role for cell differentiation state in the responsiveness of α cells. In α cells from donors with T2D, the effect of glucose on the distribution of transcriptome-wide correlations was reversed, such that high glucose associated with more positively correlated genes (Figure 2G; Table S3). GSEA of these correlations highlighted a role for cell development state in the inappropriately high α cell exocytosis at 10 mM glucose in T2D (Figure 2H). Several leading-edge transcripts enriched in these pathways, including transcription factors important for pancreatic endocrine maturity like *GATA6*, *PAX6*, *RFX6*, and *RFX3*, overlap with those that correlated with inappropriately low exocytosis in α cells of ND donors at 1 mM glucose (Figures 2F and 2I).

Glucose control of mouse α cell exocytosis and impaired "electrophysiological identity" following high-fat feeding

Following an ~10-min exposure to 1 mM glucose, depolarization of mouse islets with 20 mM KCl elicited a transient stimulation of glucagon release that was blunted in islets kept at 5 mM glucose (Figure 3A), consistent with the glucose-dependent suppression of α cell exocytosis. These differences could not be explained by the indirect paracrine effects of insulin, as insulin secretion evoked by KCl was slightly higher at 1 mM glucose than at 5 mM glucose (Figure 3B). Similar to human α cells, increasing glucose suppressed exocytosis in mouse α cells (Figure 3C). Although the physiological impact of glucose on glucagon secretion involves key paracrine signals (Briant et al., 2016), the suppression of exocytosis by increasing glucose was similar when cells were seeded at 10% of normal density (Figure 3D) and required glucose metabolism, as the non-metabolizable analog 2-deoxyglucose (2-DG) did not

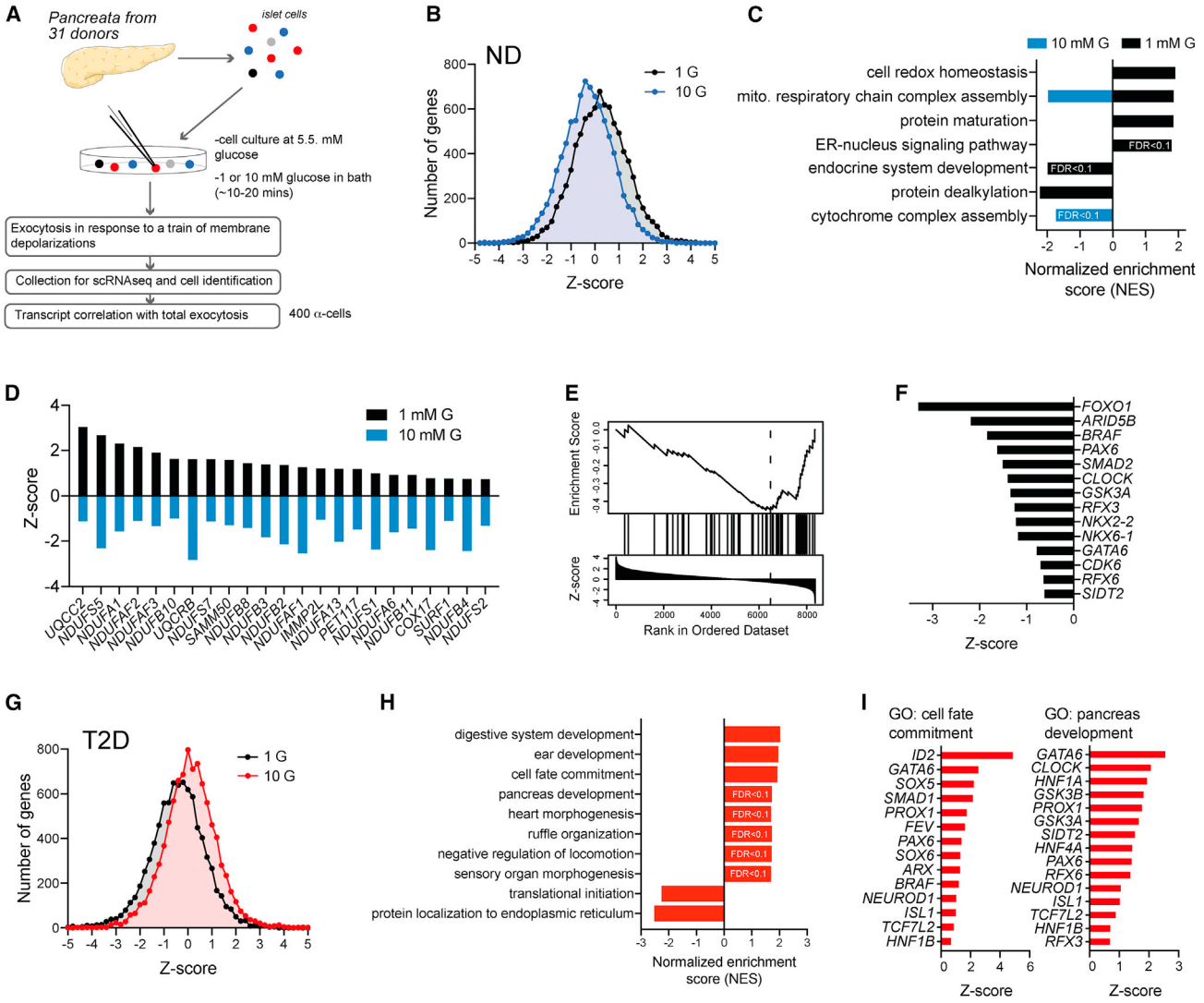

Figure 2. Patch-seq suggests roles for the mitochondrial respiratory complex in α cell function and endocrine development and cell fate in α cell dysfunction

(A) Schematic diagram illustrating the isolation of 400 α cells from 24 donors without diabetes (ND) and 7 donors with T2D assessed by patch-seq, some of which have been partly published previously (Camunas-Soler et al., 2020).

(B) The distribution of exocytosis-transcript correlations from α cells of ND donors at 1 and 10 mM glucose (see also Table S2).

(C) Gene set enrichment analysis (GSEA) Gene Ontology (GO) biological pathways using *Z* scores as weighting across the transcriptome (using genes expressed in >20% of α cells), separately at 1 and 10 mM glucose, reveal pathways linked to facilitation (positive values) or suppression (negative values) of exocytosis. FDR < 0.05 unless indicated otherwise and absence of bars indicates no significant enrichment.

(D) Leading-edge transcripts for mitochondrial respiratory chain complex assembly that flip correlation with exocytosis from positive to negative in α cells of ND donors as glucose increases from 1 to 10 mM.

(E) An endocrine system development pathway is enriched in ND α cells with low exocytotic responses at 1 mM glucose.

(F) Leading-edge genes underlying the signal in (E), which includes transcripts involved in islet cell lineage and α cell identity.

(G) The distribution of exocytosis–transcript correlations in α cells from donors with T2D at 1 and 10 mM glucose (see also Table S3).

(H) GSEA GO biological pathways with *Z* scores as weighting (using genes expressed in >20% of α cells) reveal development and cell fate pathways linked to increased exocytosis in T2D α cells at 10 mM glucose (false discovery rate [FDR] < 0.05 unless indicated otherwise).

(I) Selected leading-edge transcripts that underlie the cell fate commitment (left) and pancreas development (right) pathways, including islet lineage and α cell identity markers.

The FDRs for pathways identified by GSEA were <0.05 unless indicated otherwise.

mimic the effect of glucose (Figure 3E). The glucose suppression of Ca^{2+} entry and exocytosis could be prevented by rotenone, but not antimycin A (Figure 3F), suggesting a signal at or between mitochondrial respiratory chain complexes I and III. This could include reactive oxygen species/H_2O_2 produced by complex I via reverse electron transport (Onukwufor et al., 2019) or by complex III toward the cytosol (Muller et al., 2004). Indeed, direct intracellular dialysis of H_2O_2 suppressed

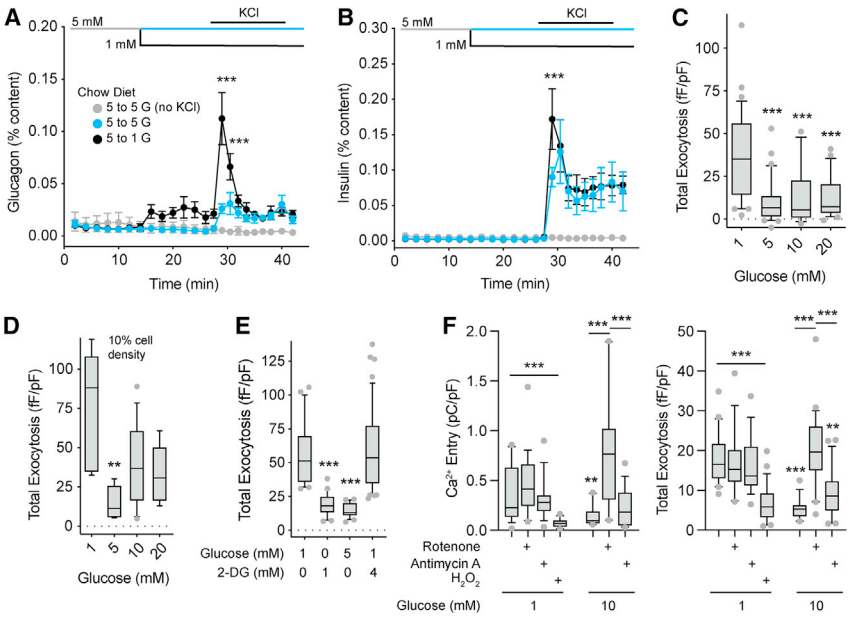

Figure 3. Glucose suppression of mouse α cell exocytosis requires glucose metabolism and the mitochondrial respiratory chain

(A and B) Glucagon (A) and insulin (B) secretion from islets of 10- to 12-week-old male C57bl6 mice as glucose remains at 5 mM (blue) or drops from 5 to 1 mM (black) and upon subsequent stimulation with 20 mM KCl. A control (gray) was maintained at 5 mM glucose (n = 3, 3, 3 mice).

(C and D) Mouse α cell exocytosis with increasing glucose (C; n = 32, 30, 14, 27 cells from 4 mice) and at very low (10% of normal) density (D; n = 6, 6, 13, 9 cells from 2 mice).

(E) Effect of 2-DG on glucose regulation of α cell exocytosis (n = 20, 20, 21, 46 cells from 4 mice).

(F) Effect of the complex I inhibitor rotenone (0.5 μM) and the complex III inhibitor antimycin A (0.5 μM) on α cell Ca^{2+} charge entry during a 500-ms depolarization from −70 to 0 mV and exocytosis at 1 and 10 mM glucose. Also the effect of direct intracellular dialysis of H_2O_2 (10 μM) via the patch pipette at 1 mM glucose (left, n = 19, 15, 18, 17, 11, 19, 16 cells; right, n = 20, 19, 16, 26, 16, 26, 22 cells from 3 mice).

**p < 0.01 and ***p < 0.001 by one-way ANOVA (C–E) or two-way ANOVA (A, B, and F), followed by Tukey post-test to compare points or groups with the 5 mM glucose points (A and B) or with the 1 mM glucose control group.

α cell Ca^{2+} influx and exocytosis in mouse (Figure 3F) and human (Figures S1E and S1F) α cells.

Low-glucose stimulation of glucagon secretion was enhanced in mice fed a high-fat diet (HFD) for 12–14 weeks compared with age-matched controls (18–20 weeks; Figure 4A), similar to what we have shown previously (Kellard et al., 2020). There was no difference in insulin secretion at 5 and 1 mM glucose but the response to high K^+ was reduced in mice fed an HFD compared with controls (Figure 4B), possibly reflecting the disruption of a direct coupling between Ca^{2+} channels and insulin granules (Collins et al., 2010). As in humans, exocytosis at 1 mM glucose in α cells from chow-fed mice was inhibited by the P/Q-type Ca^{2+} channel blocker agatoxin, but not the L-type channel blocker isradipine (Figure 4C). This was reversed in α cells from HFD mice where exocytosis is resistant to agatoxin but sensitive to isradipine (Figure 4C). Importantly, the P/Q-channel agonist GV-58, which delayed channel inactivation in α cells from both the chow-fed and HFD mice (Figure 4D), rescued exocytosis following suppression by 5 mM glucose in α cells from chow-fed but not HFD-fed mice, consistent with a loss of P/Q-type channel coupling to exocytosis (Figure 4E). Mouse α cells are distinguished from β cells by a characteristic right-shifted Na^+-current half-inactivation, and these two cell types primarily express *Scn3a* and *Scn9a*, respectively (Zhang et al., 2014). Many α cells from the HFD-fed mice, identified by glucagon immunostaining, showed a leftward shift in Na^+ channel half-inactivation toward a "β cell-like" phenotype (Figures 4F and S4A–S4C).

This switching of both Ca^{2+}-channel-exocytosis coupling and Na^+ channel half-inactivation toward "β cell-like" phenotypes upon HFD feeding is reminiscent of observations from genetically induced α to β cell trans-differentiation (Chakravarthy et al., 2017). However, the present changes occurred while glucagon expression was maintained, as the α cells were identified by glucagon immunostaining. We explored these findings in separate experiments where α cells from chow-fed and HFD-fed mice were collected for patch-seq (Figure S4A) where we confirmed the negative shift in Na^+ current inactivation (Figures S4B and S4C) and the switch from P/Q- to L-type Ca^{2+} channel dependence of exocytosis (Figure S4D). After HFD feeding some endocrine transcription factors were lower than in α cells of chow-fed mice (Figure 4G; Table S4), although there was no clear change in exocytotic or Ca^{2+} channel transcripts (Figure S4E). The β cell Na^+ channel transcript *Scn9a* was higher (Figure 4H) in α cells from HFD than chow-fed mice, and the HFD-induced shift in Na^+ channel inactivation at 1 mM glucose correlated with expression of α cell identity and islet lineage factors (Figure 4I; Table S5). Thus, after HFD feeding some α cells adopted electrophysiological properties typically associated with β cell function and a transcriptional profile consistent with altered α cell identity and/or maturation.

Electrophysiological fingerprint modeling links human α cell behavior and cell phenotype

Next, we compiled data from islet cells of 67 donors collected at 1, 5, and 10 mM glucose, identified either by scRNA-seq or immunostaining (Figure 5A). Unlike in mice, but similar to previous reports (Braun et al., 2008; Ramracheya et al., 2010), Na^+ channel properties are similar between human α and β cells and could not be reliably used alone to distinguish these cell types (Figures 5B, 5C, and S4C). In ND α cells, the peak Na^+ current significantly correlated with genes known to impact α cell activity (Figure 5D). Top positive correlates include genes involved in α cell or islet function, including Na^+ and Ca^{2+} channels (*SCN3A*, *SCN3B*, and *CACNA1A*), α and islet cell lineage transcription factors

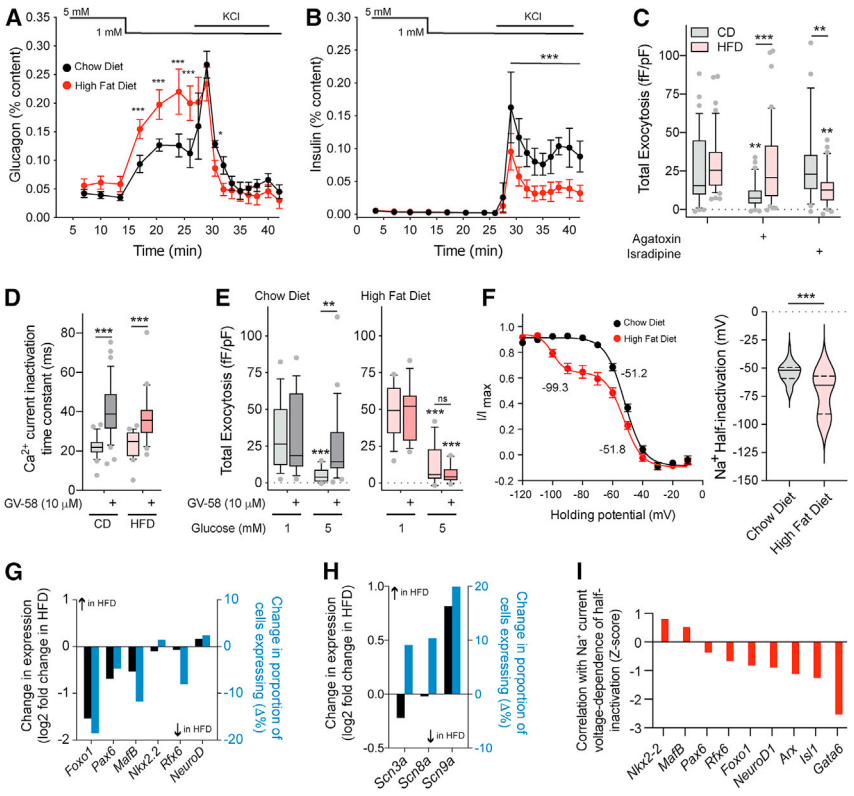

Figure 4. "β cell-like" properties of α cells from HFD-fed mice

(A and B) Glucagon (A) and insulin (B) secretion from islets of male C57/bl6N mice fed an HFD for 10–12 weeks starting from 8 weeks of age (red) compared with age matched (18–20 weeks) chow-fed controls (black) (n = 3, 3 mice).

(C) Effect of the P/Q-type Ca^{2+} channel blocker agatoxin (100 nM) and the L-type Ca^{2+} channel blocker isradipine (10 μM) on total exocytosis from chow diet (CD) and HFD α cells at 1 mM glucose (n = 34, 42, 34, 40, 29, 39 cells from 8 HFD and 8 CD mice).

(D and E) Effect of the P/Q-channel activator GV-58 (10 μM) to delay Ca^{2+} current inactivation in both CD and HFD α cells (D; n = 23, 36, 24, 23 cells from 3 CD- and 3 HFD-fed mice) and on exocytosis (E) from CD (gray) and HFD (pink) α cells at 1 and 5 mM glucose (n = 15, 16, 16, 21 cells from 3 CD-fed mice; n = 14, 13, 15, 14 cells from 3 HFD-fed mice).

(F) Steady-state voltage-dependent Na^+ current inactivation curves (left) and individual half-inactivation voltages (right) from α cells of chow-fed and HFD-fed mice (n = 36, 44 cells from 9 CD and 9 HFD mice, measured at 1 mM glucose). Half-inactivation voltages from fit curves are indicated.

(G) From a separate set of CD and HFD α cells assessed by patch-seq (Figure S4), mean expression (black) and % of cells expressing (blue) some α cell identity transcription factors in CD and HFD α cells.

(H) Mean expression (black) and % of cells expressing (blue) the β cell Na^+ channel isoform, *Scn9a*, in HFD α cells.

(I) Correlation *Z* scores of the negative shift in Na^+ channel steady-state inactivation (at 1 mM glucose) in HFD α cells with transcripts involved in α cell lineage and identity.

*p < 0.05; **p < 0.01; ***p < 0.001 by the Student's t test (F), or by one-way ANOVA (D and E) or two-way ANOVA (A–C) followed by Tukey post-test to compare points or groups with the 5 mM glucose points (A and B), with the 1 mM glucose control group, or as indicated.

(*MAFB*, *FEV*, *NKX2.2*, and *NEUROD1*), G protein-coupled receptors (*GIPR*, *SSTR1*, *FFAR1*, and *GPR119*), and secreted factors (*LOXL4*, *WNT4*, *UCN3*, and *IL16*). Negative correlates were less abundant but included the vitamin D-binding protein (*GC*), which is known to regulate α cell Na^+ currents (Viloria et al., 2020). GSEA for KEGG pathways and Gene Ontology (GO) biological process terms revealed additional pathways enriched in ND α cells with larger Na^+ currents (Figures S5A and S5B), including the serotonin, GABA, and glutamate pathways. Numerous cell surface receptor transcripts also appear as correlates to Na^+ channel activity (Figures 5E and S5C). We validated the ability of agonists of some of these to increase human α cell Na^+ currents (Figure 5F). Transcript correlates of peak Na^+ current and voltage dependence of inactivation from α cells of ND and T2D donors are provided in Table S6.

Although α cell lineage markers correlate with Na^+ currents, the overlap in Na^+ current properties between human α and β cells makes it impossible to use these alone to interrogate shifts in human α cell phenotypes. We therefore developed "electrophysiological fingerprinting" classifier models (Figure 6A) that integrate Na^+ current, Ca^{2+} current, and exocytosis measures (Figure 6B) to characterize human α cell "functional phenotypes," similar to the logistic regression (Briant et al., 2017) and random forests (Camunas-Soler et al., 2020) models that we had used previously. In those models, however, cell size was the major predictor of α cell identity. Here, we generated three independent models for cell type classification: optimizable ensemble classifiers that include (Model 1) or exclude (Model 2) cell size as an independent variable, and an extreme gradient boosting model that also excludes cell size, but with additional restrictions to donor age, donor body mass index (BMI), and organ cold ischemic time (CIT) applied to the training data (Model 3). These models distinguished ND α and β cells well (Figure 6A) and, unlike some underlying parameters, were unaffected by potential confounders, such as donor sex, BMI, CIT, cell culture time, and glucose concentration (Figure 6B).

Model output between 0 and 1 can be considered the probability an electrophysiological profile matches that of an α cell, and we called this $\alpha_{probability}$ (with $\beta_{probability} = 1 - \alpha_{probability}$). Assignment of an $\alpha_{probability}$ to all ND α and β cells for which we had patch-seq data, without *a priori* knowledge of cell type, showed the effective separation of cell types and correlation with canonical markers (Figure 6C). All three models showed a significantly reduced $\beta_{probability}$ and $\alpha_{probability}$ in β and α cells, respectively, from donors with T2D compared with cells from ND donors (Figure 6D). The expression of numerous transcripts correlated with a "loss of electrophysiological identity" in T2D α cells within one or more of the models, including lineage markers such as *ISL1*, *NEUROD1*, *FEV*, and *RFX6* (Figure 6E; Table S7). GSEA using $\alpha_{probability}$ correlation slopes as weighting for transcripts expressed

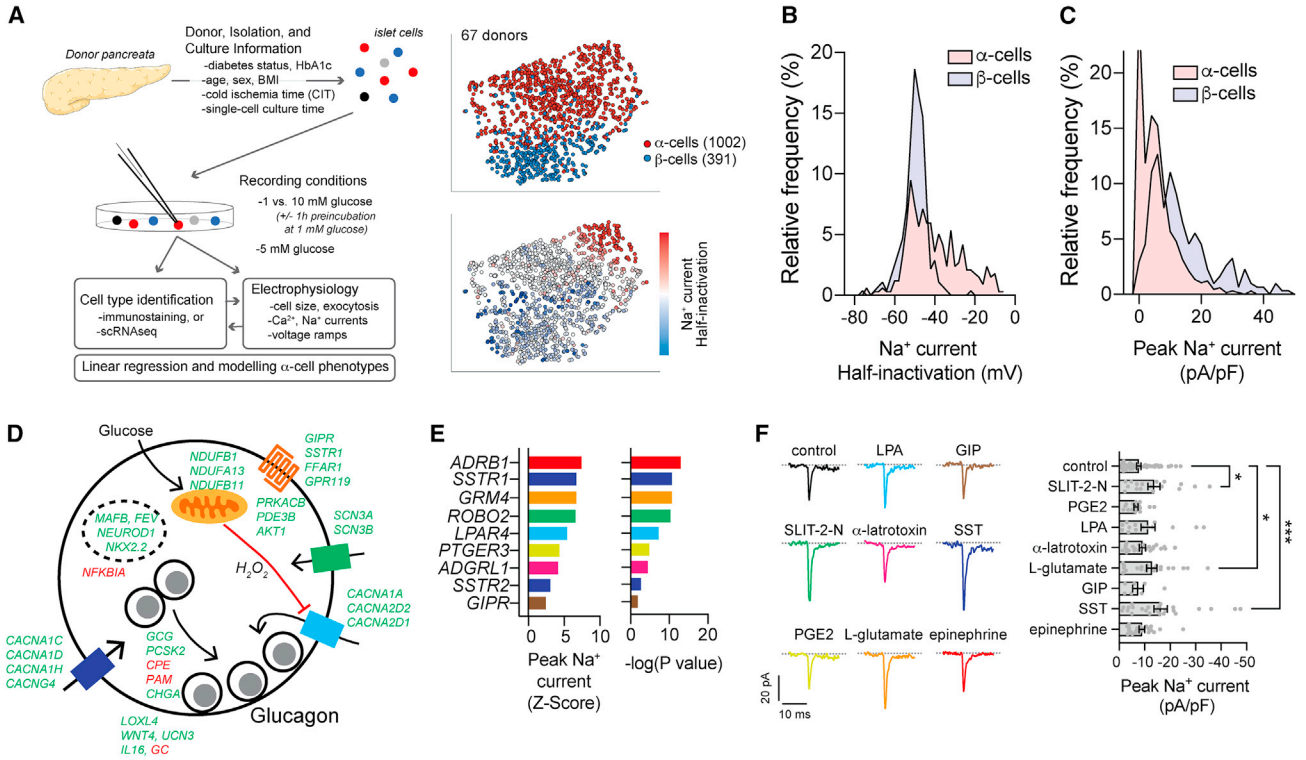

Figure 5. Na^+ current properties correlate with transcriptomic markers of α cell function

(A) Schematic diagram illustrating an expanded dataset of electrically profiled human islet cells and tSNE representations of α and β cells identified by immunostaining or sequencing along with the relative distribution of Na^+ current half-inactivation values.

(B and C) The distribution of Na^+ current amplitudes (B) and voltage-dependence of half-inactivation values (C) of β cells (light blue) and α cells (pink) (see also Figure S4C).

(D) Selected significant positive (green) and negative (red) transcript correlates of peak Na^+ current from α cells of ND donors mapped to a proposed scheme of glucose regulation of glucagon exocytosis (see also Table S6).

(E) Correlation of α cell peak Na^+ current and selected transmembrane signaling receptor transcripts (see also Figure S5).

(F) In α cells of 6 donors with no diabetes (ND), Na^+ currents measured with receptor agonists (colors matching receptors shown in E) upon depolarization from −70 to −10 mV. Peak current is shown at right: control (n = 53 cells), 0.5 μg/ml SLIT-2-N (n = 17 cells), 10 μM prostaglandin E_2 (PGE2, n = 17 cells), 0.5 μM lysophosphatidic acid (LPA, n = 14 cells), 0.2 μg/ml α-latratoxin (n = 24 cells), 10 mM L-glutamic acid (n = 21 cells), 100 nM glucose-dependent insulinotropic polypeptide (GIP, n = 7 cells), 200 nM somatostatin (SST, n = 24 cells), and 5 μM epinephrine (n = 22 cells).

*p < 0.05 and ***p < 0.001 by one-way ANOVA, followed by the Benjamini and Hochburg post-test method to compare groups controlling for false discovery rate.

in >20% of cells highlighted GO biological process terms related to mitochondrial respiratory chain complex assembly in all three models (Figure 6F), underscoring a link between increased respiratory chain complex expression and α cell dysfunction.

Impaired functional identity and exocytosis in T2D α cells enriched in lineage and immaturity markers

Human α cells exist in states of variable chromatin accessibility at the *GCG* promoter and sites enriched with transcription factor motifs characterizing endocrine lineage and development (Chiou et al., 2021). Markers of α cell lineage are heterogenous within our dataset, with evidence for increased expression in T2D (Figures 7A, S6A, and S6B). Intriguingly, this also included *ARX*, which we confirmed at the protein level, along with MAFB and glucagon itself (Figure 7B). *ARX*-enriched (*ARX*^{hi}) cells expressed consistently higher levels of progenitor transcripts like *NEUROD1*, *FEV*, *GATA6*, and others (Figure S6B). We find no difference in $\alpha_{probability}$ scores between ND α cells either enriched or deficient in these (Figures 7C and S6). In T2D, however, an impaired electrical fingerprint occurred selectively in α cells with higher levels of *ARX*, *NEUROD1*, *ISL1*, *PAX6*, *GATA6*, *FEV*, *NKX2-2*, *RFX6*, and *MAFB* (Figures 7C and S6). Accordingly, *ARX* and these other markers did not correlate with exocytosis in α cells of ND donors but did correlate significantly with impaired exocytosis in T2D (Figure 7D). In separate scRNA-seq data (Avrahami et al., 2020) we confirmed the upregulation of a juvenile α cell profile (Arda et al., 2016), tissue development genes, and a β cell-like profile selectively in *ARX*^{hi} α cells in T2D compared with α cells from ND donors (Figures 7E and S7). Finally, while the α cells with low *ISL1*, *NKX2-2*, *NEUROD1*, and *ARX* from donors with T2D had normal exocytosis at 1 mM glucose, α cells enriched in these transcripts showed impaired exocytotic function in T2D (Figure 7F).

DISCUSSION

Glucagon secretion is under the control of metabolic, paracrine, hormonal, and neuronal signals (El et al., 2020). Much

CellPress
OPEN ACCESS

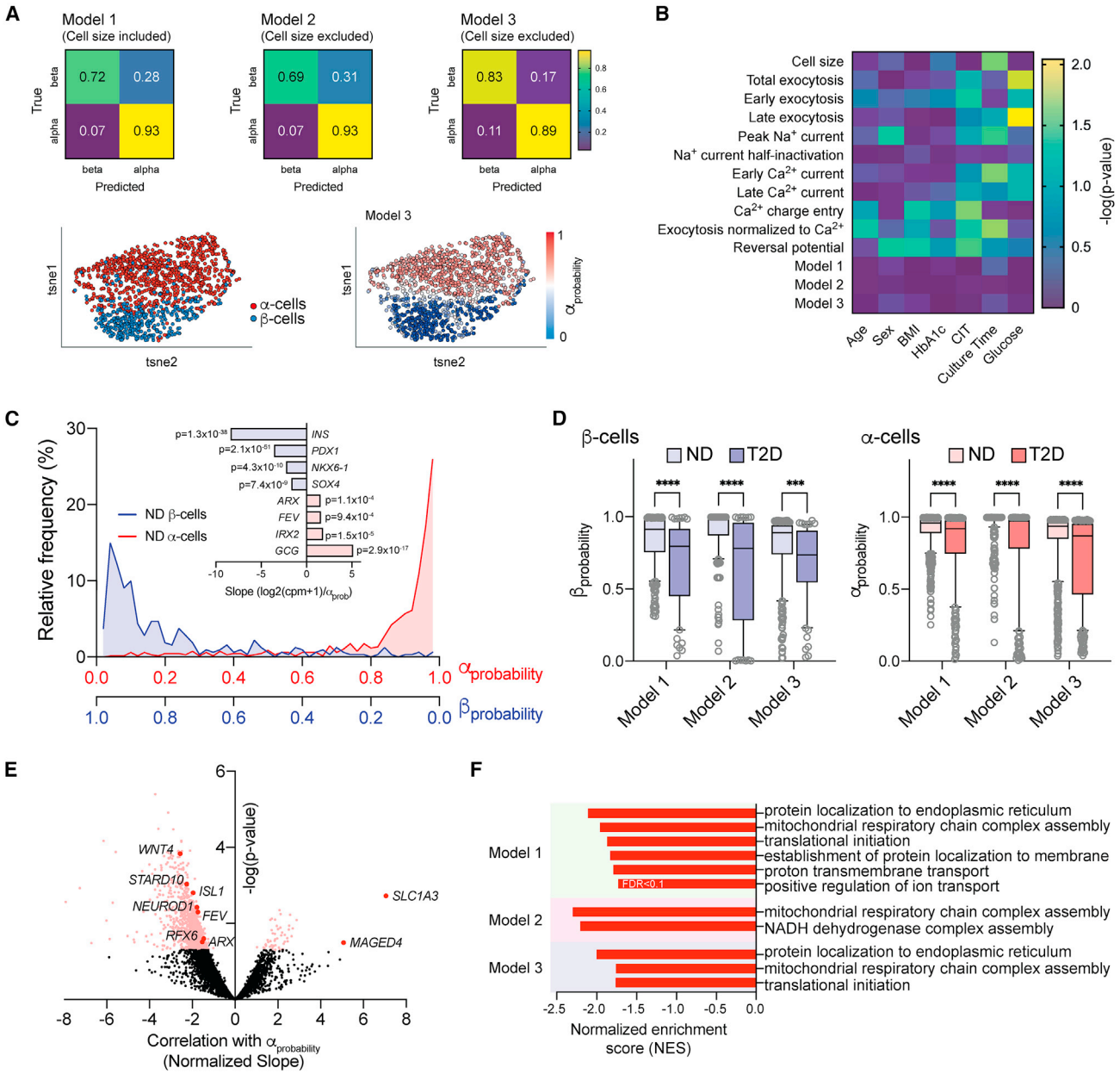

Figure 6. Electrophysiological fingerprints define a loss of "functional identity" in T2D α cells

(A) Classifier models trained on islet cell electrical properties of α and β cells from donors with no diabetes (ND) using optimizable ensemble or extreme gradient boosting (XGBoost) approaches identify cell types with high accuracy regardless of the inclusion or exclusion of cell size from training data; 80% of data was used for training; 20% of data was reserved for validation and generation of confusion matrices. tSNE plots show cell types determined by immunostaining or sequencing (left) and assigned $\alpha_{probability}$ scores (right).

(B) Ordinary least-squares multiple regression of electrophysiological properties of α cells from ND donors, model scoring, and donor/isolation variables.

(C) Calculated $\alpha_{probability}$ (and $\beta_{probability}$) values from Model 3 applied to cells collected for patch-seq, without *a priori* knowledge of cell type and correlation with canonical β cell (light blue) and α cell (pink) markers.

(D) $\beta_{probability}$ and $\alpha_{probability}$ values derived from all three models, of all β and α cells from ND or T2D donors.

(E) Volcano plot of transcript correlations with Model 3 $\alpha_{probability}$ values (slope/standard deviation) in α cells from donors with T2D. A negative correlation indicates transcripts associated with reduced $\alpha_{probability}$.

(F) Significantly enriched GO biological pathways from gene set enrichment analysis (GSEA) performed using $\alpha_{probability}$ - transcript correlation slopes of α cells from donors with T2D in all three Models as weighting.

***p < 0.001 and ****p < 0.0001 as indicated within models using non-parametric Kruskal-Wallis test (D) followed by Dunn's post-test to correct for multiple comparisons. Pink/red points in (E) indicate significance at p < 0.05. FDRs for pathways identified by GSEA in (F) were <0.05 unless indicated otherwise.

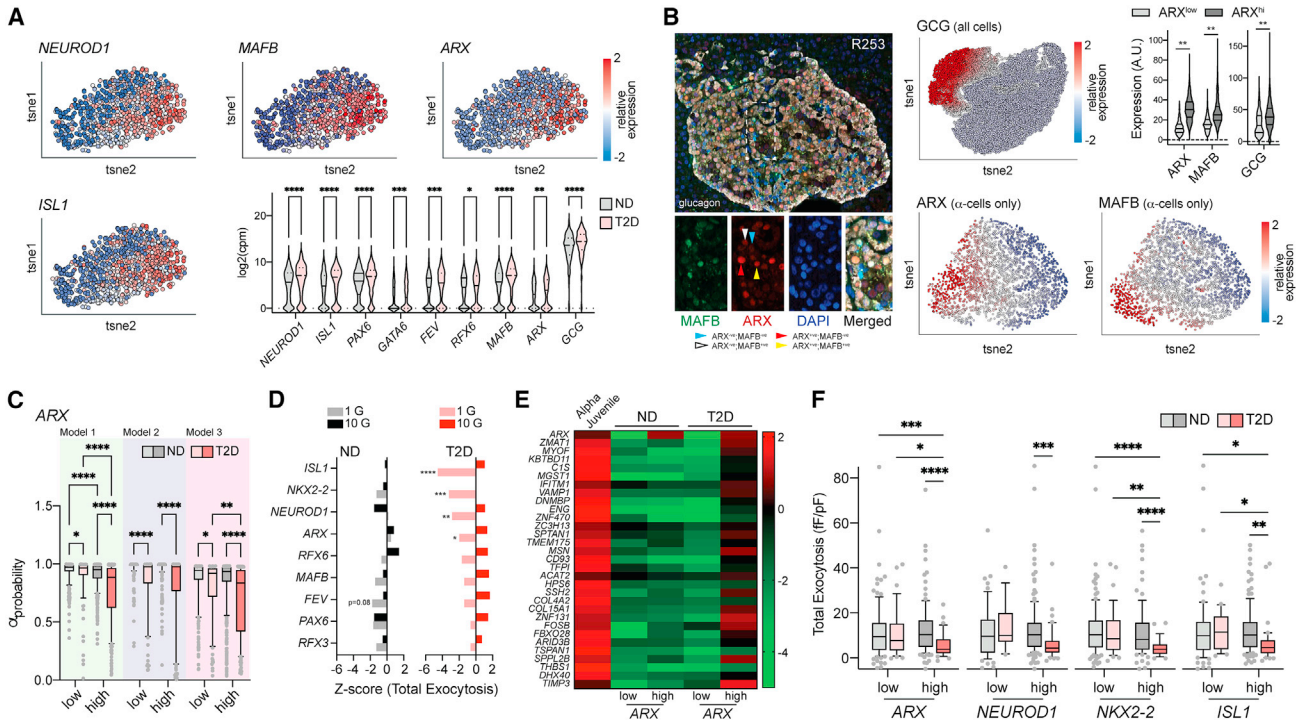

Figure 7. A role for maturation state in α cell dysfunction in T2D

(A) Heterogenous expression of transcript makers for islet cell lineage and α cell maturity in 980 patch-seq α cells.

(B) ARX and MAFB protein expression in α cells at the protein level *in situ* by immunostaining. Violin plots show the relative levels of GCG, ARX, and MAFB expressed in ARX^{low} and ARX^{hi} α cells.

(C) $\alpha_{probability}$ values from the three separate classifier models in ND and T2D α cells separated by high and low expression of *ARX* (see also Figure S6).

(D) Correlation of exocytosis in ND and T2D α cells with α cell lineage and identity markers. Bars to the left of the centerline indicate correlation with low exocytosis at the given glucose concentration.

(E) In a separate human islet single-cell dataset (Avrahami et al., 2020), expression of a juvenile α cell gene set in ND and T2D α cells separated by low and high *ARX* expression. The heatmap displays relative expression levels as median $\log_2$ FPKM values.

(F) Total exocytosis in ND and T2D α cells at 1 mM glucose separated by low and high expression of *ISL1*, *NEUROD1*, *NKX2-2*, and *ARX*.

*p < 0.05; **p < 0.01; ***p < 0.001; ****p < 0.0001 by two-way ANOVA followed by two-stage step-up method for estimation of FDR (C, D, and F) or Tukey post-test (B).

debate has centered on the question of whether glucose suppression of glucagon secretion is mediated via intrinsic, paracrine, or autonomic mechanisms (Gylfe, 2016), although it seems likely that α cells (like β cells) adeptly integrate multiple signals for precise physiologic control of glucagon. A role for direct glucose sensing is supported by the ability of glucose to modulate α cell ATP-sensitive K^+ channels (Zhang et al., 2013), the impact of α cell glucokinase manipulation on *in vitro* cell function, and *in vivo* glucagon secretion and glucose homeostasis (Moede et al., 2020; Bahl et al., 2021; Basco et al., 2018). Here, we show that glucose suppresses human and mouse α cell exocytosis, consistent with a recent report where exocytosis was measured by live-cell imaging (Omar-Hmeadi et al., 2020). A role for α cell metabolism is supported by the effect of the non-metabolizable glucose analog 2-DG and the correlation of responses with mitochondrial respiratory complex assembly transcripts, particularly those of complex 1. Indeed, the ability of rotenone to block glucose suppression of α cell Ca^{2+} currents and exocytosis suggests a signaling role for reactive oxygen species and H_2O_2 generated by complex I. Consistent with this, intracellular application of H_2O_2 mimics the effect of glucose while reduced glutathione blocks the effect of glucose, and external H_2O_2 inhibits low-glucose-stimulated glucagon secretion (Allister et al., 2013).

The study by Omar-Hmeadi et al. (2020) showed a U-shaped response of isolated α cells to glucose, suggesting that glucose may increase α cell exocytosis under some conditions. We found some hints of this in our own data, including in α cells of donors with T2D. In ND α cells this may depend on the culture conditions. Following prolonged low-glucose preincubation α cells were larger, possibly due to continued glucagon granule fusion. Subsequent exocytotic responses were smaller when the α cells were maintained at 1 mM glucose, while acute glucose-stimulation then increased exocytosis. This is reminiscent of the glucose-dependent increase in glucagon secretion from purified α cells (Olsen et al., 2005). Thus, glucose acutely suppresses P/Q-type Ca^{2+} channels via a complex-I-dependent mechanism to limit depolarization-induced α cell exocytosis, while at the same time facilitating glucagon granule priming or docking to maintain the availability of granules. Altogether, these processes will "tune" α cell responsiveness to a myriad of paracrine, endocrine, and neuronal inputs.

The P/Q-type Ca^{2+} current seen at low glucose in α cells of ND donors appears absent in T2D but channel expression is not reduced; therefore, channel regulation appears disrupted. It seems possible that altered mitochondrial function in α cells in T2D could drive dysregulation of P/Q-type Ca^{2+} channel activity, and indeed, mitochondrial dysfunction has been demonstrated in α cells from hyperglycemic mice (Knudsen et al., 2019) and mitochondrial morphology is altered in α cells from Western-diet-fed mice (Grubelnik et al., 2020). Genes involved in glucose metabolism appear downregulated in α cells from donors with type 1 diabetes (Brissova et al., 2018), although these may exhibit a more extreme phenotype than in T2D, with downregulation of several channels, exocytotic transcripts, and α cell identity markers. We do find an upregulation, particularly in *ARX*^{hi} T2D α cells, of mitochondrial respiratory chain complex assembly transcripts and a clear correlation of this with the impaired α cell phenotype by fingerprint modeling; however, a demonstration of altered mitochondrial respiratory function and/or reactive oxygen species generation in α cells from donors with T2D remains to be shown.

The coupling of glucagon exocytosis to P/Q-type Ca^{2+} channels, which we confirmed at low glucose, has been demonstrated previously (De Marinis et al., 2010; Ramracheya et al., 2010) and is similar to the direct coupling of insulin granule exocytosis to the activation of L-type Ca^{2+} channels (Wiser et al., 1999). These and other electrophysiological properties are used to distinguish α and β cells in rodents. Most commonly, mouse islet cell types are identified by a combination of cell size (α cells are smaller) and distinct properties of Na^+ current inactivation. In a model of genetically induced α-to-β trans-differentiation in mice, we reported a clear shift in electrophysiological phenotype consistent with the attainment of β cell properties (Chakravarthy et al., 2017). Intriguingly, following high-fat feeding, mouse α cells undergo a negative shift in Na^+ current inactivation and convert from P/Q- to L-type Ca^{2+} channel dependence of exocytosis. While we provide some evidence for impaired α cell identity, this is not associated with a clear transdifferentiation, as β cell markers are not increased and cells maintain positive immunostaining for glucagon. The shift in Na^+ channel inactivation toward a "β cell-like" phenotype, which could be related to changes in membrane composition (Godazgar et al., 2018), correlates with the expression of important α cell lineage and identity transcription factors, suggesting that the change in electrical phenotype occurs more readily in cells with higher levels of these markers.

A subset of human α cells, even from donors without diabetes, exist in an immature state and may suffer a further loss of mature identity in T2D (Avrahami et al., 2020), perhaps related to their greater epigenetic plasticity (Bramswig et al., 2013) and distinct states of chromatin accessibility (Chiou et al., 2021). We find that α cells from ND donors with inappropriately low exocytosis are enriched in transcripts and pathways associated with endocrine development (*FOXO1*, *PAX6*, *RFX6*, and others). In T2D we see no obvious loss of α cell transcription factors or upregulation of β cell-defining transcription factors indicative of trans-differentiation per se. We do, however, find heterogeneity in many lineage markers, as reported previously by us (Camunas-Soler et al., 2020; Drigo et al., 2019) and by others (Li et al., 2016). In our dataset, most of these show a small but significant increase in T2D. To assess a shift in electrophysiological phenotype of these human α cells we could not use Na^+ current inactivation alone, as this feature overlaps with measurements from human β cells. We therefore modified machine-learning approaches that we used previously to improve the identification of mouse (Briant et al., 2017) and human (Camunas-Soler et al., 2020) islet cells. We used exocytosis, Na^+ current, and Ca^{2+} properties as training data for three separate models with similar results. Two of these excluded cell size to solely identify shifts in membrane "activity," and all models accurately assigned probability values for α and β cells irrespective of ambient glucose, culture times, and other important donor- and isolation-related parameters. Correlation of $\alpha_{probability}$ values with transcriptomic data therefore emphasized pathways linked to a "loss of functional phenotype" in T2D and suggests that α cells with the most altered electrical phenotypes in T2D are those with higher expression of pancreatic endocrine lineage markers.

In this study, we define an impaired α cell phenotype in T2D that is largely restricted to a subgroup of cells expressing higher levels of markers that define not only α cell maturity but pancreatic endocrine lineage. At first look we would have expected that high levels of *ARX* should be indicative of mature α cell function but this is misleading given a strong overlap of *ARX*^{hi} cells with transcripts more traditionally associated with an endocrine progenitor state such as *NEUROD1*, *ISL1*, *FEV*, and others. These cells indeed appear more "plastic" in their electrophysiological responses, which may predispose them to an altered electrical phenotype in T2D. We confirm in a separate dataset the "de-repression" of immature gene sets associated with a "juvenile" α cell phenotype and with tissue development restricted to *ARX*^{hi} α cells in T2D. Thus, we demonstrate that all α cells are not equally impacted by disease and that a subset of α cells defined by their maturation state may be key drivers of impaired glucagon responses in T2D.

Limitations of study

While tempting to link impaired exocytosis in α cells from donors with T2D to an impaired responsiveness to hypoglycemia *in vivo*, this must be considered in the context of *in situ* α cell function, which will be impacted by the local environment and by paracrine or hormonal signals. Here, we studied single isolated α cells, and although we demonstrate a similar heterogeneity in ARX/MAFB protein expression *in situ*, α cell function may be different within the intact pancreas and would likely be impacted by architectural changes in the disease state. Encouragingly though, we find clear differences between ND and T2D α cells that persist *in vitro*, and among the novel findings of this study we also find well-established regulators of α cell function (such as *GIPR*). Additionally, both α cell function and transcript expression are likely dynamic and impacted by metabolic status or culture conditions. Indeed, preculture at low glucose can alter α cell exocytotic function. Our approach to "electrophysiological fingerprinting" addresses this in part since it is unaffected by glucose, time in single-cell culture (up to 3 days), or various donor-related parameters. Nonetheless, the relevance of possible dynamic shifts in α cell phenotype in T2D remains unclear. We do not know, for example, if exocytotic function would be restored if T2D α cells transition from an *ARX*^{hi} to *ARX*^{lo} state or whether such a transition itself is impaired.

While α cells enriched in lineage factors appear less mature and maintain some plasticity, whether T2D induces a true reversal of maturation or a more general phenotypic drift could still be questioned. While an enrichment of numerous gene sets including β cell genes in the *ARX*^{hi} cells in T2D could suggest the latter, we note that those are also all enriched in true juvenile α cells (Avrahami et al., 2020). The exact links between these changes and dysregulated glucagon secretion remains somewhat speculative, particularly since we see no decrease in Ca^{2+} channel transcripts to explain the reduced Ca^{2+} currents. Interestingly, mitochondrial respiratory complex assembly transcripts are increased in T2D α cells, most notably in the α cells with impaired function and enriched for *ARX*. While altered mitochondrial function could drive P/Q-type Ca^{2+} channel inhibition and impaired exocytosis, and we provide some evidence linking the respiratory chain to α cell dysfunction in T2D, we do not know if mitochondrial respiration is altered in T2D α cells. This will require assessment of mitochondrial function and oxygen consumption in the *ARX*^{hi} subset of α cells from donors with T2D as a future priority.

Finally, we should be careful when directly comparing the rodent and human studies. One clear difference we find is that human α cells in T2D show impaired (low) exocytosis at 1 mM glucose and a modest increase with higher glucose, while the mouse HFD α cells instead show altered Na^{+} channel inactivation and exocytosis-Ca^{2+}-channel coupling. The exact reasons for these differences are unclear but perhaps related to obvious differences between humans and the mouse model (disease/HFD duration, degree of dysglycemia, age, etc.). Nonetheless, in both mice and human cells, we find evidence to suggest that α cell dysfunction is linked to cell maturation state.

STAR★METHODS

Detailed methods are provided in the online version of this paper and include the following:

- KEY RESOURCES TABLE
- RESOURCE AVAILABILITY
  - Lead contact
  - Materials availability
  - Data and code availability
- EXPERIMENTAL MODEL AND SUBJECT DETAILS
  - Human islets
  - Mouse islets
- METHOD DETAILS
  - Patch-clamp recordings
  - Pancreas patch-seq
  - Hormone secretion measurements
  - Immunostaining and single-cell protein analysis
  - Gene-set and pathway analysis of scRNA-seq
- QUANTIFICATION AND STATISTICAL ANALYSIS
  - Electrophysiological fingerprint Modeling
  - Statistical analysis

SUPPLEMENTAL INFORMATION

Supplemental information can be found online at https://doi.org/10.1016/j.cmet.2021.12.021.

ACKNOWLEDGMENTS

The University of Alberta is situated on Treaty 6 territory, traditional lands of First Nations and Métis people. We thank Dr. Jesper Grud Skat Madsen (University of Southern Denmark), Dr. Jakob Knudsen (University of Copenhagen), and Dr. Lori Sussel (University of Colorado) for helpful discussion and Dr. Francis Lynn (University of British Columbia) for critical reading of the draft manuscript. We thank the Human Organ Procurement and Exchange (HOPE) program and Trillium Gift of Life Network (TGLN) for their work in procuring human donor pancreas for research. We also thank Dr. Rita Bottino (Allegheny Health Network) and Drs. James Shapiro and Tatsuya Kin (University of Alberta Clinical Islet Program) for contributing some islet preparations for this study. Finally, we especially thank the organ donors and their families for their kind gift in support of diabetes research. T.d.S. was supported by the Alberta-Helmholtz Diabetes Research School, the Alberta Innovates Scholarship in Data-Enabled Innovation, and the Sir Fredrik Banting and Dr. Charles Best Canada Graduate Scholarship. This work was funded by grants to P.E.M. from the Canadian Institutes of Health Research (CIHR; 148451); from the JDRF to P.E.M., L.B., and P.R. (SRA-2019-698-S-B); and from the National Institutes of Health (F32 DK109577 to E.M.W.; R01 DK126482 to R.S., P.E.M., and S.K.; and U01 DK120447 to P.E.M., R.A.D., and S.K.). Some islet samples were from the Human Pancreas Analysis Program (HPAP; RRID: SCR_016202), a Human Islet Research Network (RRID: SCR_014393) consortium (UC4-DK-112217 and UC4-DK-112232). P.E.M. holds the Canada Research Chair in Islet Biology.

AUTHOR CONTRIBUTIONS

X.-Q.D., J.C.-S., A.B., A.F.S., T.d.S., L.J.J.B., A.N., R.A.D., E.M.W., D.A., J.J., and R.C.J. collected and analyzed data. J.L., N.S., A.B., and J.E.M.F. isolated human islets. P.E.L., K.H.K., S.K.K., S.R.Q., P.R., R.W.S., and P.E.M. conceived the study, designed experiments, and analyzed data. P.E.M. wrote the initial manuscript draft and all authors contributed to editing the final version. P.E.M. acts as the guarantor of this work and is responsible for data access.

DECLARATION OF INTERESTS

The authors declare no competing interests.

Received: April 9, 2021
Revised: October 8, 2021
Accepted: December 22, 2021
Published: February 1, 2022

REFERENCES

Allister, E.M., Robson-Doucette, C.A., Prentice, K.J., Hardy, A.B., Sultan, S., Gaisano, H.Y., Kong, D., Gilon, P., Herrera, P.L., Lowell, B.B., and Wheeler, M.B. (2013). UCP2 regulates the glucagon response to fasting and starvation. Diabetes *62*, 1623–1633.

Anders, S., Pyl, P.T., and Huber, W. (2015). HTSeq—a Python framework to work with high-throughput sequencing data. Bioinformatics *31*, 166–169.

Arda, H.E., Li, L., Tsai, J., Torre, E.A., Rosli, Y., Peiris, H., Spitale, R.C., Dai, C., Gu, X., Qu, K., and Wang, P. (2016). Age-dependent pancreatic gene regulation reveals mechanisms governing human β cell function. Cell Metab *23*, 909–920.

Avrahami, D., Wang, Y.J., Schug, J., Feleke, E., Gao, L., Liu, C., HPAP Consortium, Naji, A., Glaser, B., and Kaestner, K.H. (2020). Single-cell transcriptomics of human islet ontogeny defines the molecular basis of β-cell dedifferentiation in T2D. Mol. Metab. *42*, 101057.

Bahl, V., Lee May, C.L., Perez, A., Glaser, B., and Kaestner, K.H. (2021). Genetic activation of α-cell glucokinase in mice causes enhanced glucose-suppression of glucagon secretion during normal and diabetic states. Mol. Metab. *49*, 101193.

Bankhead, P., Loughrey, M.B., Fernández, J.A., Dombrowski, Y., McArt, D.G., Dunne, P.D., McQuaid, S., Gray, R.T., Murray, L.J., Coleman, H.G., and

James, J.A. (2017). QuPath: open source software for digital pathology image analysis. Sci. Rep. *7*, 16878.

Barg, S., Galvanovskis, J., Göpel, S.O., Rorsman, P., and Eliasson, L. (2000). Tight coupling between electrical activity and exocytosis in mouse glucagon-secreting alpha-cells. Diabetes *49*, 1500–1510.

Barg, S., Ma, X., Eliasson, L., Galvanovskis, J., Göpel, S.O., Obermüller, S., Platzer, J., Renström, E., Trus, M., Atlas, D., et al. (2001). Fast exocytosis with few Ca(2+) channels in insulin-secreting mouse pancreatic B cells. Biophys. J. *81*, 3308–3323.

Basco, D., Zhang, Q., Salehi, A., Tarasov, A., Dolci, W., Herrera, P., Spiliotis, I., Berney, X., Tarussio, D., Rorsman, P., and Thorens, B. (2018). α-cell glucokinase suppresses glucose-regulated glucagon secretion. Nat. Commun. *9*, 546.

Bokvist, K., Eliasson, L., Ammälä, C., Renström, E., and Rorsman, P. (1995). Co-localization of L-type Ca^{2+} channels and insulin-containing secretory granules and its significance for the initiation of exocytosis in mouse pancreatic B-cells. EMBO J *14*, 50–57.

Bramswig, N.C., Everett, L.J., Schug, J., Dorrell, C., Liu, C., Luo, Y., Streeter, P.R., Naji, A., Grompe, M., and Kaestner, K.H. (2013). Epigenomic plasticity enables human pancreatic α to β cell reprogramming. J. Clin. Invest. *123*, 1275–1284.

Braun, M., Ramracheya, R., Bengtsson, M., Zhang, Q., Karanauskaite, J., Partridge, C., Johnson, P.R., and Rorsman, P. (2008). Voltage-gated ion channels in human pancreatic beta-cells: electrophysiological characterization and role in insulin secretion. Diabetes *57*, 1618–1628.

Briant, L., Salehi, A., Vergari, E., Zhang, Q., and Rorsman, P. (2016). Glucagon secretion from pancreatic α-cells. Ups. J. Med. Sci. *121*, 113–119.

Briant, L.J.B., Zhang, Q., Vergari, E., Kellard, J.A., Rodriguez, B., Ashcroft, F.M., and Rorsman, P. (2017). Functional identification of islet cell types by electrophysiological fingerprinting. J. R. Soc. Interface *14*, 20160999.

Brissova, M., Haliyur, R., Saunders, D., Shrestha, S., Dai, C., Blodgett, D.M., Bottino, R., Campbell-Thompson, M., Aramandla, R., Poffenberger, G., and Lindner, J. (2018). α cell function and gene expression are compromised in type 1 diabetes. Cell Rep *22*, 2667–2676.

Camunas-Soler, J., Dai, X.Q., Hang, Y., Bautista, A., Lyon, J., Suzuki, K., Kim, S.K., Quake, S.R., and MacDonald, P.E. (2020). Patch-seq links single-cell transcriptomes to human islet dysfunction in diabetes. Cell Metab *31*, 1017–1031.e4.

Chakravarthy, H., Gu, X., Enge, M., Dai, X., Wang, Y., Damond, N., Downie, C., Liu, K., Wang, J., Xing, Y., and Chera, S. (2017). Converting adult pancreatic islet α cells into β cells by targeting both Dnmt1 and Arx. Cell Metab *25*, 622–634.

Chiou, J., Zeng, C., Cheng, Z., Han, J.Y., Schlichting, M., Miller, M., Mendez, R., Huang, S., Wang, J., Sui, Y., and Deogaygay, A. (2021). Single-cell chromatin accessibility identifies pancreatic islet cell type– and state-specific regulatory programs of diabetes risk. Nat. Genet. *53*, 455–466.

Collins, S.C., Hoppa, M.B., Walker, J.N., Amisten, S., Abdulkader, F., Bengtsson, M., Fearnside, J., Ramracheya, R., Toye, A.A., Zhang, Q., and Clark, A. (2010). Progression of diet-induced diabetes in C57BL6J mice involves functional dissociation of Ca2(+) channels from secretory vesicles. Diabetes *59*, 1192–1201.

Dai, X.Q., Spigelman, A.F., Khan, S., Braun, M., Manning Fox, J.E.M., and MacDonald, P.E. (2014). SUMO1 enhances cAMP-dependent exocytosis and glucagon secretion from pancreatic α-cells. J. Physiol. *592*, 3715–3726.

De Marinis, Y.Z.D., Salehi, A., Ward, C.E., Zhang, Q., Abdulkader, F., Bengtsson, M., Braha, O., Braun, M., Ramracheya, R., Amisten, S., and Habib, A.M. (2010). GLP-1 inhibits and adrenaline stimulates glucagon release by differential modulation of N- and L-type Ca^{2+} channel-dependent exocytosis. Cell Metab *11*, 543–553.

Dobin, A., Davis, C.A., Schlesinger, F., Drenkow, J., Zaleski, C., Jha, S., Batut, P., Chaisson, M., and Gingeras, T.R. (2013). STAR: ultrafast universal RNA-seq aligner. Bioinformatics *29*, 15–21.

Drigo, R.A.e., Erikson, G., Tyagi, S., Capitanio, J., Lyon, J., Spigelman, A.F., Bautista, A., Fox, J.E.M., Shokhirev, M., MacDonald, P.E., and Hetzer, M.W. (2019). Aging of human endocrine pancreatic cell types is heterogeneous and sex-specific. bioRxiv. https://doi.org/10.1101/729541.

El, K., Capozzi, M.E., and Campbell, J.E. (2020). Repositioning the alpha cell in postprandial metabolism. Endocrinology *161*, bqaa169.

Ferdaoussi, M., Dai, X., Jensen, M.V., Wang, R., Peterson, B.S., Huang, C., Ilkayeva, O., Smith, N., Miller, N., Hajmrle, C., and Spigelman, A.F. (2015). Isocitrate-to-SENP1 signaling amplifies insulin secretion and rescues dysfunctional β cells. J. Clin. Invest. *125*, 3847–3860.

Gembal, M., Gilon, P., and Henquin, J.C. (1992). Evidence that glucose can control insulin release independently from its action on ATP-sensitive K^+ channels in mouse B cells. J. Clin. Invest. *89*, 1288–1295.

Girard, J. (2017). Glucagon, a key factor in the pathophysiology of type 2 diabetes. Biochimie *143*, 33–36.

Godazgar, M., Zhang, Q., Chibalina, M.V., and Rorsman, P. (2018). Biphasic voltage-dependent inactivation of human NaV1.3, 1.6 and 1.7 Na^+ channels expressed in rodent insulin-secreting cells. J. Physiol. *596*, 1601–1626.

Göpel, S.O., Kanno, T., Barg, S., Weng, X.G., Gromada, J., and Rorsman, P. (2000). Regulation of glucagon release in mouse -cells by K_{ATP} channels and inactivation of TTX-sensitive Na^+ channels. J. Physiol. *528*, 509–520.

Grubelnik, V., Markovič, R., Lipovšek, S., Leitinger, G., Gosak, M., Dolenšek, J., Valladolid-Acebes, I., Berggren, P.O., Stožer, A., Perc, M., and Marhl, M. (2020). Modelling of dysregulated glucagon secretion in type 2 diabetes by considering mitochondrial alterations in pancreatic α-cells. R. Soc. Open Sci. *7*, 191171.

Gylfe, E. (2016). Glucose control of glucagon secretion-'There's a brand-new gimmick every year. Ups. J. Med. Sci. *121*, 120–132.

Huang, Y.C., Gaisano, H.Y., and Leung, Y.M. (2011a). Electrophysiological identification of mouse islet α-cells: from isolated single α-cells to in situ assessment within pancreas slices. Islets *3*, 139–143.

Huang, Y.C., Rupnik, M., and Gaisano, H.Y. (2011b). Unperturbed islet α-cell function examined in mouse pancreas tissue slices. J. Physiol. *589*, 395–408.

Kaestner, K.H., Powers, A.C., Naji, A., and Atkinson, M.A. (2019). NIH initiative to improve understanding of the pancreas, islet, and autoimmunity in type 1 diabetes: the Human Pancreas Analysis Program (HPAP). Diabetes *68*, 1394–1402.

Kellard, J.A., Rorsman, N.J.G., Hill, T.G., Armour, S.L., Bunt, M. van de, Rorsman, P., Knudsen, J.G., and Briant, L.J.B. (2020). Reduced somatostatin signalling leads to hypersecretion of glucagon in mice fed a high-fat diet. Mol. Metab. *40*, 101021.

Kim, J., Okamoto, H., Huang, Z., Anguiano, G., Chen, S., Liu, Q., Cavino, K., Xin, Y., Na, E., Hamid, R., and Lee, J. (2017). Amino acid transporter Slc38a5 controls glucagon receptor inhibition-induced pancreatic α cell hyperplasia in mice. Cell Metab *25*, 1348–1361.e8.

Knudsen, J.G., Hamilton, A., Ramracheya, R., Tarasov, A.I., Brereton, M., Haythorne, E., Chibalina, M.V., Spégel, P., Mulder, H., Zhang, Q., and Ashcroft, F.M. (2019). Dysregulation of glucagon secretion by hyperglycemia-induced sodium-dependent reduction of ATP production. Cell Metab *29*, 430–442.e4.

Korsunsky, I., Millard, N., Fan, J., Slowikowski, K., Zhang, F., Wei, K., Baglaenko, Y., Brenner, M., Loh, P.R., and Raychaudhuri, S. (2019). Fast, sensitive and accurate integration of single-cell data with Harmony. Nat. Methods *16*, 1289–1296.

Lam, C.J., Cox, A.R., Jacobson, D.R., Rankin, M.M., and Kushner, J.A. (2018). Highly proliferative α-cell-related islet endocrine cells in human pancreata. Diabetes *67*, 674–686.

Le Marchand, S.J.L., and Piston, D.W. (2010). Glucose suppression of glucagon secretion: metabolic and calcium responses from alpha-cells in intact mouse pancreatic islets. J. Biol. Chem. *285*, 14389–14398.

Li, J., Klughammer, J., Farlik, M., Penz, T., Spittler, A., Barbieux, C., Berishvili, E., Bock, C., and Kubicek, S. (2016). Single-cell transcriptomes reveal characteristic features of human pancreatic islet cell types. EMBO Rep *17*, 178–187.

Liao, Y., Wang, J., Jaehnig, E.J., Shi, Z., and Zhang, B. (2019). WebGestalt 2019: gene set analysis toolkit with revamped UIs and APIs. Nucleic Acids Res *47*, W199–W205.

Lyon, J., Kin, T., Bautista, A., Smith, N., MacDonald, P., and Manning, J. (2019). Isolation of human pancreatic islets of Langerhans for research v3. Protocols.Io. https://doi.org/10.17504/protocols.io.bt55nq86.

Matsuoka, T.A., Kawashima, S., Miyatsuka, T., Sasaki, S., Shimo, N., Katakami, N., Kawamori, D., Takebe, S., Herrera, P.L., Kaneto, H., and Stein, R. (2017). Mafa enables Pdx1 to effectively convert pancreatic islet progenitors and committed islet α-cells into β-cells in vivo. Diabetes *66*, 1293–1300.

Moede, T., Leibiger, B., Vaca Sanchez, P.V., Daré, E., Köhler, M., Muhandiramlage, T.P., Leibiger, I.B., and Berggren, P.O. (2020). Glucokinase intrinsically regulates glucose sensing and glucagon secretion in pancreatic alpha cells. Sci. Rep. *10*, 20145.

Muller, F.L., Liu, Y., and Van Remmen, H.V. (2004). Complex III releases superoxide to both sides of the inner mitochondrial membrane. J. Biol. Chem. *279*, 49064–49073.

Olsen, H.L., Theander, S., Bokvist, K., Buschard, K., Wollheim, C.B., and Gromada, J. (2005). Glucose stimulates glucagon release in single rat α-cells by mechanisms that mirror the stimulus-secretion coupling in β-cells. Endocrinology *146*, 4861–4870.

Omar-Hmeadi, M., Lund, P.E., Gandasi, N.R., Tengholm, A., and Barg, S. (2020). Paracrine control of α-cell glucagon exocytosis is compromised in human type-2 diabetes. Nat. Commun. *11*, 1896.

Onukwufor, J.O., Berry, B.J., and Wojtovich, A.P. (2019). Physiologic implications of reactive oxygen species production by mitochondrial complex I reverse electron transport. Antioxidants (Basel) *8*, 285.

Pedregosa, F., Varoquaux, G., Gramfort, A., Michel, V., Thirion, B., Grisel, O., Blondel, M., Prettenhofer, P., Weiss, R., Dubourg, V., and Vanderplas, J. (2012). Scikit-learn: machine learning in Python. J. Mach. Learn. Res. *12*, 2825–2830.

Picelli, S., Faridani, O.R., Björklund, A.K., Winberg, G., Sagasser, S., and Sandberg, R. (2014). Full-length RNA-seq from single cells using Smart-seq2. Nat. Protoc. *9*, 171–181.

Ramracheya, R., Chapman, C., Chibalina, M., Dou, H., Miranda, C., González, A., Moritoh, Y., Shigeto, M., Zhang, Q., Braun, M., and Clark, A. (2018). GLP-1 suppresses glucagon secretion in human pancreatic alpha-cells by inhibition of P/Q-type Ca^{2+} channels. Physiol. Rep. *6*, e13852.

Ramracheya, R., Ward, C., Shigeto, M., Walker, J.N., Amisten, S., Zhang, Q., Johnson, P.R., Rorsman, P., and Braun, M. (2010). Membrane potential-dependent inactivation of voltage-gated ion channels in alpha-cells inhibits glucagon secretion from human islets. Diabetes *59*, 2198–2208.

Reissaus, C.A., and Piston, D.W. (2017). Reestablishment of glucose inhibition of glucagon secretion in small pseudoislets. Diabetes *66*, 960–969.

Sato, Y., Aizawa, T., Komatsu, M., Okada, N., and Yamada, T. (1992). Dual functional role of membrane depolarization/Ca^{2+} influx in rat pancreatic B-cell. Diabetes *41*, 438–443.

Seabold, S., and Perktold, J. (2010). Statsmodels: econometric and statistical modeling with Python. Proceedings of the 9th Python in Science Conf *57*, 61.

Shuai, H., Xu, Y., Yu, Q., Gylfe, E., and Tengholm, A. (2016). Fluorescent protein vectors for pancreatic islet cell identification in live-cell imaging. Pflugers Arch *468*, 1765–1777.

Smith, N., Spigelman, A., Lin, H., and MacDonald, P.E. (2020). Mouse pancreatic islet isolation. Protocols.Io. https://doi.org/10.17504/protocols.io.sqaedse.

Stoltzfus, C.R., Filipek, J., Gern, B.H., Olin, B.E., Leal, J.M., Wu, Y., Lyons-Cohen, M.R., Huang, J.Y., Paz-Stoltzfus, C.L., Plumlee, C.R., and Pöschinger, T. (2020). CytoMAP: A spatial analysis toolbox reveals features of myeloid cell organization in lymphoid tissues. Cell Rep *31*, 107523.

Subramanian, A., Tamayo, P., Mootha, V.K., Mukherjee, S., Ebert, B.L., Gillette, M.A., Paulovich, A., Pomeroy, S.L., Golub, T.R., Lander, E.S., et al. (2005). Gene set enrichment analysis: A knowledge-based approach for interpreting genome-wide expression profiles. Proc. Natl. Acad. Sci. U. S. A. *102*, 15545–15550.

Tarr, T.B., Valdomir, G., Liang, M., Wipf, P., and Meriney, S.D. (2012). New calcium channel agonists as potential therapeutics in Lambert–Eaton myasthenic syndrome and other neuromuscular diseases. Ann. N. Y. Acad. Sci. *1275*, 85–91.

Thorel, F., Népote, V., Avril, I., Kohno, K., Desgraz, R., Chera, S., and Herrera, P.L. (2010). Conversion of adult pancreatic alpha-cells to beta-cells after extreme beta-cell loss. Nature *464*, 1149–1154.

van der Meulen, T., Mawla, A.M., DiGruccio, M.R., Adams, M.W., Nies, V., Dólleman, S., Liu, S., Ackermann, A.M., Cáceres, E., Hunter, A.E., and Kaestner, K.H. (2017). Virgin beta cells persist throughout life at a neogenic niche within pancreatic islets. Cell Metab *25*, 911–926.e6.

Viloria, K., Nasteska, D., Briant, L.J.B., Heising, S., Larner, D.P., Fine, N.H.F., Ashford, F.B., da Silva Xavier, G.da S., Ramos, M.J., Hasib, A., and Mesirov, J.P. (2020). Vitamin-D-binding protein contributes to the maintenance of α cell function and glucagon secretion. Cell Rep *31*, 107761.

Wiser, O., Trus, M., Hernández, A., Renström, E., Barg, S., Rorsman, P., and Atlas, D. (1999). The voltage sensitive Lc-type Ca^{2+} channel is functionally coupled to the exocytotic machinery. Proc. Natl. Acad. Sci. U. S. A. *96*, 248–253.

Zadeh, E.H.G., Huang, Z., Xia, J., Li, D., Davidson, H.W., and Li, W.-H. (2020). ZIGIR, a granule-specific Zn^{2+} indicator, reveals human islet α cell heterogeneity. Cell Rep *32*, 107904.

Zhang, Q., Ramracheya, R., Lahmann, C., Tarasov, A., Bengtsson, M., Braha, O., Braun, M., Brereton, M., Collins, S., Galvanovskis, J., and Gonzalez, A. (2013). Role of K_{ATP} channels in glucose-regulated glucagon secretion and impaired counterregulation in type 2 diabetes. Cell Metab *18*, 871–882.

Zhang, Q., Chibalina, M.V., Bengtsson, M., Groschner, L.N., Ramracheya, R., Rorsman, N.J.G., Leiss, V., Nassar, M.A., Welling, A., Gribble, F.M., and Reimann, F. (2014). Na^{+} current properties in islet α- and β-cells reflect cell-specific Scn3a and Scn9a expression. J. Physiol. *592*, 4677–4696.

STAR★METHODS

KEY RESOURCES TABLE

REAGENT or RESOURCE	SOURCE	IDENTIFIER
Antibodies		
Insulin Antibody (H-86)	Santa Cruz	SC-9168; RRID: AB_2126540
Anti-Glucagon Antibody, clone 13D11.33	EMD Millipore	MABN238; RRID: AB_433707
Goat anti-Guinea Pig IgG (H+L) Highly Cross-Adsorbed Secondary Antibody, Alexa Fluor 594	ThermoFisher Scientific	A-11076; RRID: AB_141930
Monoclonal Anti-Glucagon antibody produced in mouse	Sigma-Aldrich	G2654; RRID: AB_259852
Human ARX Affinity Purified Polyclonal Ab antibody	R&D Systems	AF7068; RRID: AB_10973178
MAFB Antibody	Cell Signaling Technology	41019; RRID: AB_2799192
Cy3-AffiniPure Goat Anti-Mouse IgG	Jackson ImmunoResearch	115-165-003; RRID: AB_2338680
Cy2-AffiniPure Goat Anti-Rabbit IgG	Jackson ImmunoResearch	111-225-144, RRID: AB_2338021
Cy5-AffiniPure Donkey Anti-Sheep IgG	Jackson ImmunoResearch	713-175-147, RRID: AB_2340730
Biological samples		
Human pancreatic islets	Alberta Diabetes Institute IsletCore	See Table S1
Human pancreatic islets	University of Alberta Clinical Islet Laboratory	See Table S1
Human pancreatic islets	Allegheny Health Network	See Table S1
Human pancreatic islets	Human Pancreas Analysis Program	See Table S1
Chemicals, peptides, and recombinant proteins		
RPMI 1640 media	ThermoFisher Scientific	11875
low glucose DMEM media	ThermoFisher Scientific	11885
Fetal Bovine Serum - Canadian origin	ThermoFisher Scientific	12483020
Bovine Serum Albumin	Sigma-Aldrich	A6003
Penicillin-Streptomycin	ThermoFisher Scientific	15070063
StemPro Accutase Cell Dissociation Reagent	ThermoFisher Scientific	A1110501
chemicals/salts for patch-clamp and KRB buffers	Sigma-Aldrich	N/A
isradipine	Sigma-Aldrich	I6658
agatoxin	Alomone Labs	STA-500
GV-58	Alomone Labs	G-140
rotenone	Sigma-Aldrich	R8875
antimycin A	Sigma-Aldrich	A8674
lysophosphatidic acid	Sigma-Aldrich	L7260
alpha-latrotoxin	Enzo Life Sciences	ALX-630-027-C040
SLIT-2-N human	Sigma-Aldrich	SRP3155
prostaglandin E2	Tocris	2296
somatostatin	Sigma-Aldrich	S9129
GIP, rat	Eurogentec	AS-65568
L-glutamic acid	Sigma-Aldrich	G1251
epinephrine	Sigma-Aldrich	E4375
LIVE/DEAD Fixable near-IR dead cell dye	Life Technologies	L10119
ERCC spike-in control	ThermoFisher Scientific	4456740
5X All-In-One RT Master Mix	Applied Biological Materials	G486
10% Triton	Sigma-Aldrich	93443

(*Continued on next page*)

Continued

REAGENT or RESOURCE	SOURCE	IDENTIFIER
Recombination RNase inhibitor	Clontech	2313A
SUPERase-In RNase Inhibitor	ThermoFisher Scientific	AM2696
10 mM dNTP	ThermoFisher Scientific	18427088
DAPI Fluoromount-G	SouthernBiotech	0100-20
Critical commercial assays		
U-PLEX Mouse Glucagon Assay	Meso Scale Diagnostics	K1525YK
STELLUX Rodent Insulin Chemiluminescence ELISA	ALPCO	80-INSMR-CH10
KAPA HiFi HotStart ReadyMix	KAPA Biosystems	KK2601
Nextera XT	Illumina	FC-131-1096
Deposited data		
Single cell mRNA-seq data	this paper	GEO: GSE164875
Single cell mRNA-seq data	Camunas-Soler et al., 2020	GEO: GSE124742
Single cell mRNA-seq data	Avrahami et al., 2020	GEO: GSE154126
Processed patch-seq datasets	Camunas-Soler et al., 2020	https://github.com/jcamunas/patchseq
Experimental models: Organisms/strains		
mouse C57BL/6NCrl Inbred	Charles River Laboratories	CRL:027; RRID: IMSR_CRL:027
5L0D Picolab Laboratory Rodent Diet	LabDiet	3005659-220
Mouse Diet, High Fat Calories	VWR / Bio-Serv	CA89067-471
Oligonucleotides		
SmartSeq2 OligodT: 5'–AAGCAGTGGTATCAACGCAGAGT ACT30VN-3'	Picelli et al., 2014	N/A
SmartSeq2 TSO: 5'-AAGCAGTGGTATCAACGCAGAGTA CATrGrG-3'	Picelli et al., 2014	N/A
SmartSeq2 ISPCR: 5'-AAGCAGTGGTATCAACGCAGAGT-3'	Picelli et al., 2014	N/A
Software and algorithms		
Qlucore Omics Explorer v3.6	Qlucore	https://www.qlucore.com/
WEB-based Gene SeT AnaLysis Toolkit	Liao et al., 2019	http://webgestalt.org/
Graphpad Prism v9.0.0	GraphPad	https://www.graphpad.com
Custom analysis software	Camunas-Soler et al., 2020	https://github.com/jcamunas/patchseq
PatchMaster 2x90.1	Smart Ephys HEKA	https://www.heka.com
FitMaster 2x90.1	Smart Ephys HEKA	https://www.heka.com
STAR	Dobin et al., 2013	https://github.com/alexdobin/STAR
HTSeq	Anders et al., 2015	https://github.com/simon-anders/htseq
MATLAB R2020a	Mathworks	https://uk.mathworks.com/products/matlab.html
Qupath v0.2.3	Bankhead et al., 2017	https://qupath.github.io
Cytomap v1.4	Stoltzfus et al., 2020	https://gitlab.com/gernerlab/cytomap
Genomica	Segal Lab of Computational Biology	http://genomica.weizmann.ac.il/
GSEA 4.1.0	Subramanian et al., 2005	http://software.broadinstitute.org/gsea/index.jsp
Python v3.7.11	Python Software Foundation	http://www.python.org
XGBoost v1.0.2	XGBoost	https://xgboost.readthedocs.io/en/latest/python/index.html
Scikit-learn v0.24.2	Pedregosa et al., 2012	https://scikit-learn.org/stable/
Statsmodel v0.12.2	Seabold and Perktold, 2010	https://www.statsmodels.org/stable/index.html

RESOURCE AVAILABILITY

Lead contact

Further information and requests for resources and reagents should be directed to and will be fulfilled by the lead contact, Patrick MacDonald (pmacdonald@ualberta.ca).

Materials availability

This study did not generate new unique reagents.

Data and code availability

Raw sequencing reads are available in the NCBI Gene Expression Omnibus (GEO) and Sequence Read Archive (SRA) under accession numbers GSE124742 and GSE164875.

The code and scripts generated during this study, as well as preprocessed datasets, are available at https://github.com/jcamunas/patchseq.

Data S1 represents an Excel file containing the values that were used to create all the graphs in the paper. Any additional information required to reanalyze the data reported in this paper is available from the lead contact upon request.

EXPERIMENTAL MODEL AND SUBJECT DETAILS

Human islets

In most cases, human islets were from our in-house human islet isolation and distribution program (https://www.isletcore.ca) (Lyon et al., 2019). Some human islets were provided by the Clinical Islet Transplant Program at the University of Alberta, by Dr. Rita Bottino at the Alleghany Health Network (Pennsylvania, US), or from the Human Pancreas Analysis Program (Kaestner et al., 2019). Details of donors with no diabetes (ND) or type 2 diabetes (T2D) used in this study are shown in Table S1. T2D was determined either by reporting of previous clinical diagnosis at the time of organ procurement, or by assessment of %HbA1c > 6.5 in a few cases that were considered as previously undiagnosed T2D. Human islets and dispersed cells were cultured in DMEM (ThermoFisher, #11885) with 10% FBS (ThermoFisher, #12483020) and 100 U/ml penicillin/streptomycin (Thermo Fisher, #15070063) at 37°C and 5% CO_2. In our previous study (Camunas-Soler et al., 2020) we saw no obvious effect of sex on patch-seq data, or when analyses were corrected for sex as a co-variate. In the present study we find that electrophysiological fingerprint modelling is not impacted by donor sex (Figure 6B). All donors provided written informed consent for research. Human tissue studies were approved by the Human Research Ethics Board of the University of Alberta (Pro00013094, Pro00001754).

Mouse islets

Mouse islets were isolated from chow-fed (5L0D Picolab Laboratory Rodent Diet, #3005659-220) male C57bl/6N mice (Charles River, #CRL:027; RRID: IMSR_CRL:027) at 10-12 weeks of age or following 10-12 weeks of high fat diet (60% of calories from fat; VWR Bio-Serv, #CA89067-471) starting from 8 weeks of age by collagenase digestion and hand-picking (Smith et al., 2020). Mouse islets and dispersed cells were cultured in RPMI (ThermoFisher, #11875) with 10% FBS and 100 U/ml penicillin/streptomycin at 37°C and 5% CO_2. Animals were housed at 20-24°C with a 12h:12h light:dark cycle and daily health checks. Studies were performed in accordance with institutional guidelines and were approved by the Animal Care and Use Committee at the University of Alberta (AUP00000291).

METHOD DETAILS

Patch-clamp recordings

Hand-picked islets were dissociated to single cells using StemPro accutase (Thermo Fisher, #A1110501). Dispersed islet cells were cultured for 1–3 days, after which media was changed to bath solution containing (in mM): 118 NaCl, 20 TEA, 5.6 KCl, 1.2 $MgCl_2$, 2.6 $CaCl_2$, 5 HEPES, and with glucose as indicated (pH adjusted to 7.4 with NaOH) in a heated chamber (32–35 °C). Modulators of Ca^{2+} channels (isradipine, Sigma-Aldrich, # I6658; agatoxin, Alomone Labs, #STA-500; GV-58, Alomone Labs, #G-140) or mitochondrial respiratory chain inhibitors (antimycin A, Sigma-Aldrich, #A8674; rotenone, Sigma-Aldrich, #R8875) were added to the bath, and pH adjusted, as indicated in figure legends. For whole-cell patch-clamping, fire polished thin wall borosilicate pipettes coated with Sylgard (3–5 MOhm) contained intracellular solution (in mM): 125 Cs-glutamate, 10 CsCl, 10 NaCl, 1 $MgCl_2$, 0.05 EGTA, 5 HEPES, 0.1 cAMP and 3 MgATP (pH adjusted to 7.15 with CsOH). Electrophysiological measurements were collected using a HEKA EPC10 amplifier and PatchMaster Software (SmartEphys HEKA) within 5 minutes of break-in as described previously (Camunas-Soler et al., 2020). Quality control was assessed stability of the seal (>10 GOhm) and access resistance. Cells were identified by post-hoc immunostaining for insulin with a rabbit anti-insulin primary antibody (Santa Cruz; #SC-9168; RRID: AB_2126540) and goat anti-rabbit Alexa Fluor 488 secondary (ThermoFisher, #A-11076; RRID: AB_141930), and with a guinea pig anti-glucagon primary antibody (Sigma-Aldrich, #G2654; RRID: AB_259852) and goat anti-guinea pig Alexa Fluor 594 secondary (ThermoFisher, #A-11076; RRID: AB_141930); or following collection for single-cell RNA sequencing analysis (Camunas-Soler et al., 2020).

For assessment of Ca^{2+} channel activity using Ba^{2+} as a charge carrier (Figures 1C and 1F) bath solution contained (in mM): 100 NaCl, 20 $BaCl_2$, 5 CsCl, 1 $MgCl_2$, 10 HEPES, with 0.2 μM tetrodotoxin and glucose as indicated (pH 7.4 with NaOH); and intracellular solution was (in mM): 140 Cs-glutamate, 1 $MgCl_2$, 20 TEA, 5 EGTA, 20 HEPES, 3 Mg-ATP (pH 7.15 with CsOH). For validation of receptor agonist effects on Na^+ currents (Figure 5F), bath solution contained (in mM): 118 NaCl, 20 TEA, 5.6 KCl, 1.2 $MgCl_2$, 5 HEPES, and 5 mM glucose (pH 7.4 with NaOH); and intracellular solution was (in mM): 125 Cs-glutamate, 10 CsCl, 10 NaCl, 1 $MgCl_2$, 0.05 EGTA, 5 HEPES (pH 7.15 with CsOH). Compounds used were: lysophosphatidic acid (LPA; Sigma-Aldrich, #L7260), α-latrotoxin (Enzo Life Sciences, #ALX-630-027-C040), Slit guidance ligand 2 (SLIT-2-N; Sigma-Aldrich, #SRP3155), prostaglandin E_2 (PGE2; Tocris, #2296), somatostatin (SST; Sigma-Aldrich, #S9129), glucose-dependent insulinotropic polypeptide (GIP; Eurogentec, #AS-65568), L-glutamic acid (Sigma-Aldrich, #G1251), and epinephrine (Sigma-Aldrich, #E4375). These were added in bath solution, at the concentrations indicated in the figure legend, and pH was re-adjusted if needed. Na^+ current was activated by a 50 ms depolarization from -70 to -10 mV.

Pancreas patch-seq

Our protocol for pancreas patch-seq is outlined in a recent paper (Camunas-Soler et al., 2020). In brief, following patch-clamp cells were collected using a separate wide-bore collection pipette (0.2-0.5 MOhm) filled with lysis buffer (10% Triton, Sigma-Aldrich, #93443; ribonuclease inhibitor 1:40, Clontech, #2313A), ERCC RNA spike-in mix (1:600000; ThermoFisher, #4456740), 10 mM dNTP, and 100 μM dT (3'-AAGCAGTGGTATCAACGCAGAGTACTTTTTTTTTTTTTTTTTTTTTTTTTTTTVN-5′) and then transferred to PCR tubes and stored at -80°C. We generated cDNA and sequencing libraries using an adaption of the SmartSeq-2 protocol for patch-seq plates (Camunas-Soler et al., 2020; Picelli et al., 2014). Libraries were generated from the amplified cDNA by tagmentation with Tn5 and sequenced in the NovaSeq platform (Illumina) using paired-end reads (100 bp) to an average depth of 1 million reads per cell. Sequencing reads were aligned to the human genome (GRCh38 genome with supplementary ERCC sequences) using STAR (Dobin et al., 2013), and gene counts determined using htseq-count (intersection-nonempty) using a GTF annotation with Ensembl 89 release genes (Anders et al., 2015). Gene expression was normalized to counts per million (cpm) after removal of counts corresponding to ERCC spike-ins and transformed to $\log_2$ values after addition of a pseudocount. This was followed by QC filtering of the sequenced cells (Camunas-Soler et al., 2020) to remove low-quality cells and potential doublets. Raw sequencing reads are available in the NCBI Gene Expression Omnibus (GEO) and Sequence Read Archive (SRA) under accession numbers GSE124742 and GSE164875. Correlation between transcript expression and electrophysiology was as outlined previously (Camunas-Soler et al., 2020). Visualization as t-distributed stochastic neighbor embedding (tSNE) plots was with the Qlucore Omics Explorer v3.6. Gene-set enrichment analysis (GSEA) was performed with of Z-scores or slopes for transcripts found in >20% of cells using the WEB-based Gene SeT AnaLysis Toolkit (http://webgestalt.org/) and weighted set gene coverage to reduce redundancy in identified terms (Liao et al., 2019).

Hormone secretion measurements

Groups of 150-175 hand-picked mouse islets were perifused using a BioRep perifusion system (BioRep, Miami). Islets were pre-incubated in perfused KRB buffer containing (in mM): 140 NaCl, 3.6 KCl, 2.6 $CaCl_2$, 0.5 NaH_2PO_4, 0.5 $MgSO_4$, 5 HEPES, 2 $NaHCO_3$ and 0.5 mg/ml Essentially fatty acid free BSA (Sigma A6003) for 30 minutes, and then perifused in the same KRB with changes in glucose and KCl as indicated. Samples were collected at 90 -210 sec intervals and stored for assay of glucagon (U-PLEX Mouse Glucagon Assay, Meso Scale Diagnostics, #K1525YK) and insulin (STELLUX Rodent Insulin Chemiluminescence ELISA, ALPCO, #80-INSMR-CH10) at -20°C.

Immunostaining and single-cell protein analysis

Human paraffin embedded pancreas biopsies were sectioned to 3 μm and immunostained with antibodies against MAFB (Cell Signaling Technologies, #41019; RRID:AB_2799192), ARX (R&D Systems, # AF7068; RRID:AB_10973178) and GCG (Sigma-Aldrich, #G2654; RRID:AB_259852). The secondary antibodies were Cy2, Cy3, or Cy5 conjugated (1:500; Jackson ImmunoResearch, 111-225-144, RRID:AB_2338021; 115-165-003; RRID:AB_2338680, 713-175-147, RRID:AB_2340730). Nuclear co-staining was conducted with DAPI Fluoromount G (Southern Biotech, #0100-20). Immunofluorescent mages were acquired on a Zeiss Axio Imager M2 widefield microscope with ApoTome. Images containing islet and exocrine cells were processed for nuclei segmentation, individual cell detection and cytosol border inference using Qupath software v0.2.3 (Bankhead et al., 2017). Parameters for nuclei detection: background radius 20px, median filter 5px, sigma 7px, minimum nuclei area 10px^2, maximum nuclei area 1000px^2, threshold of 2, nuclei were split by shape, and cell boundaries were determined by an expansion threshold of 12px with smoothing. Next, the relative expression levels of nuclear ARX, nuclear MAFB and cytosolic GCG levels for each detected cell were exported as.csv files and imported into Cytomap v1.4 for spatial analysis (Stoltzfus et al., 2020). In Qlucore Omics Explorer v3.6, we performed dimensionality reduction using tSNE of all imaged islet dataset using default parameters with 30 perplexity and 0.5 theta. Data was normalized for each dataset and the relative GCG, ARX and MAFB levels were displayed in the tSNE plot. Next, we created a gate to select the α-cell population in our dataset and the relative levels of ARX and MAFB were plotted. This information was used to determine the identity of ARX^{hi} and ARX^{low} cells and the relative expression levels of ARX, MAFB and GCG for each α-cell subpopulation was plotted.

Gene-set and pathway analysis of scRNA-seq

To characterize the expression program of *ARX*^{hi} and *ARX*^{low} α-cells in ND and T2D samples, we conducted gene set enrichment analysis (GSEA) on aggregated *ARX*^{hi} versus *ARX*^{low} α-cell transcriptomes from our recently published data (Avrahami et al., 2020) using a hypergeometric test by Genomica software (http://genomica.weizmann.ac.il/) considering gene sets with a p value < 0.01 and an FDR <0.05 to be significantly enriched. Pathway analyses were performed with Gene Set Enrichment Analysis (GSEA) (Subramanian et al., 2005).

QUANTIFICATION AND STATISTICAL ANALYSIS

Electrophysiological fingerprint Modeling

Multiple regression was carried out on ND α-cells using Ordinary Least Squared (OLS) Regression with Statsmodel v0.12.2 (Seabold and Perktold, 2010). Independent variables included age, sex, body mass index (BMI), HbA1c, cold ischemia time (CIT), culture time, and glucose concentration. Dependent variables included: cell size (pF), total exocytosis (fF/pF), early exocytosis (fF/pF), late exocytosis (fF/pF), peak Na^+ current (pA/pF), Na^+ half-Inactivation (mV), early Ca^{2+} current (pA/pF), late Ca^{2+} current (pA/pF), Ca^{2+} charge entry during an initial depolarization (pC/pF), exocytosis normalized to Ca^{2+} charge entry (fF/pC), reversal potential (mV), and $\alpha_{probability}$ from Models 1-3 (see below). Cells lacking data for a dependent variable were only dropped from that specific OLS analysis. Classification of cell type was conducted using the above electrophysiological measures as dependent variables from ND donors in an Optimizable Ensemble that either included (Model 1) or excluded (Model 2) cell size in MATLAB, or using Extreme Gradient Boosting (XGBoost v1.0.2) in a Python v3.7.11 framework that excluded cell size and reversal potential and restricted training data to 32 ND donors within an age of 20-70 years, a BMI of 18.5-30.3, and a pancreas CIT of $\leq$20 hours. Fine tuning was performed with a pre-determined minimum accuracy of 80% for both α- and β-cells and training was performed with early stopping set to 50 iterations and utilized AUCPR as the evaluation metric. Models were trained on 80% of the α- and β-cells, with 20% reserved for testing and validation. Confusion matrices were generated using scikit-learn v0.24.2 (Pedregosa et al., 2012). We applied the models across our combined immunostaining and patch-seq database of ND and T2D cells and utilized the classifier's predicted probability scores to assess fit to α-cell ($\alpha_{probability}$ = 1.0) and β-cell ($\alpha_{probability}$ = 0.0) models.

Statistical analysis

Data are expressed as mean and standard error (line plots), mean and 10-90 percentile range (box and whisker plots), or as violin plots with median and quartiles indicated. When comparing two groups we used Student's t test or the non-parametric Mann-Whitney test to compare ranks. When comparing more than two groups we used one-way or two-way ANOVA followed by either the Tukey post-test or two-stage step-up method for estimation of false discovery rate (FDR); or alternatively the non-parametric Kruskal-Wallis test followed by Dunn's post-test to correct for multiple comparisons. Statistical tests used are indicated in the figure legends. p values less than 0.05 were considered as significant. For correlation of electrophysiology with transcript expression, Spearman tie-corrected correlations were computed for each gene and significance was tested by bootstrapping (1,000 iterations) as described in our previous work (Camunas-Soler et al., 2020). For ORA and GSEA, false discovery rate (FDR) of reported pathways was <0.05 or <0.1 as indicated in the figures using Bengamini-Hochberg (BH) correction within the WEB-based GEne SeT AnaLysis Toolkit (webgestalt.org). We did not perform power calculations prior to experiments, and experimenters were not blinded. Animals were assigned randomly to CD and HFD groups, and all human donors were accepted for islet isolations if they met the requirement for negative serology reports. No cells that passed standard electrophysiology and sequencing quality control (described above) were excluded from analysis.